

Statistical study of the energetic proton environment at Titan's orbit from the Cassini spacecraft

L. H. Regoli^{1,2,3,4}, E. Roussos¹, K. Dialynas⁵, J. G. Luhmann⁶, N. Sergis⁵, X. Jia², D. Román²,
A. Azari², N. Krupp¹, G. H. Jones^{3,4}, A. J. Coates^{3,4} and I. J. Rae³

¹Max Planck Institute for Solar System Research, Göttingen, Germany.

²Climate and Space Sciences and Engineering, University of Michigan, Ann Arbor, USA.

³Mullard Space Science Laboratory, University College London, Holmbury St. Mary, UK.

⁴Centre for Planetary Science at UCL/Birkbeck, London, UK.

⁵Office for Space Research and Technology, Academy of Athens, Greece.

⁶Space Sciences Laboratory, University of California, Berkeley, USA.

Key Points:

- Energetic particle environment at Titan's orbit highly variable
- Ion data present SLT asymmetry with higher fluxes in the pre-midnight sector
- Derivation of empirical model of ion spectra based on Kappa distribution function

This is the author manuscript accepted for publication and has undergone full peer review but has not been through the copyediting, typesetting, pagination and proofreading process, which may lead to differences between this version and the [Version of Record](#). Please cite this article as doi: [10.1029/2018JA025442](https://doi.org/10.1029/2018JA025442)

Corresponding author: Leonardo Regoli, lregoli@umich.edu

Abstract

A statistical study of the energetic proton environment at Titan's orbit as captured by the MIMI/LEMMS and MIMI/CHEMS instruments is performed. The data analyzed cover all the dedicated flybys of Titan by Cassini as well as the orbit crossings that happen far from the moon. The energetic environment is found to be highly variable on timescales comparable to that of the duration of a flyby. Analysis of H^+ ion fluxes reveals a weak asymmetry in Saturn local time (SLT) with the highest fluxes occurring in the pre-midnight sector of the magnetosphere. A correlation between the energetic ion fluxes and the location of Cassini in the magnetosphere with respect to the center of the current sheet can be observed. Finally, an empirical model of proton spectra for energies above 20 keV is derived based on fits to Kappa distribution functions. This model can be used to better understand the interaction of Titan with the magnetosphere and the energy deposition by energetic particles below the main ionospheric peak.

1 Introduction

The interaction of Titan with its surrounding environment is arguably one of the most complex interactions of its kind in the Solar System. The mean orbital distance of the moon to Saturn is 20.3 Saturn radii (R_S), which locates it close to the magnetopause stand-off distance, described using a bimodal model with mean distances of 22 and 27 R_S by *Achilleos et al.* [2008], when crossing the sub-solar point. As a consequence, while Titan spends most of the time in the outer region of the Saturnian magnetosphere, under strong solar wind conditions it can be located within the magnetosheath [*Bertucci et al.*, 2008; *Edberg et al.*, 2013] or in the unshocked solar wind [*Bertucci et al.*, 2015].

Titan's orbit lies almost at the equator but due to the fact that Saturn's current sheet can move up and down into a bowl shape due to solar wind activity [*Arridge et al.*, 2008], the moon can be located inside or outside the plasma sheet at any given time. This flapping motion of the current sheet, affected by magnetospheric dynamics, can be faster than the transit time of Cassini during dedicated flybys. This, together with the different trajectory geometries for different flybys makes it possible for the plasma and field instruments to detect different plasma environments during the inbound and outbound parts of the trajectory [*Simon et al.*, 2013].

Since Titan does not possess an internal magnetic field [*Backes et al.*, 2005; *Wei et al.*, 2010], its atmosphere and ionosphere interact directly with the different environments just described, creating a unique moon-magnetosphere interaction when located inside the magnetosphere. When located upstream of the Saturnian bow shock, the interaction is very similar to that of Mars [e.g. *Brecht and Ledvina*, 2006; *Brain et al.*, 2010] or Venus [e.g. *Slavin et al.*, 1980; *Russell et al.*, 2006] with the solar wind [*Bertucci et al.*, 2015]. When located in the magnetosheath, Titan has been observed to retain signatures of the Saturnian magnetic field in the conducting ionosphere, something that has been referred to in the literature as fossil fields [*Bertucci et al.*, 2008].

During the Cassini era, it became clear that the north-south orientation of the magnetic field observed during the Voyager 1 flyby [*Neubauer et al.*, 1984] was not common, with only a single flyby reported in the literature, namely T70 [*Simon et al.*, 2013], having occurred during such conditions. For this reason, different efforts to classify the different environments at which Titan can be located have been undertaken using different data sets provided by different instruments on board Cassini.

Using electron data from the Electron Spectrometer (ELS), part of the Cassini Plasma Spectrometer (CAPS), and from the Low Energy Magnetospheric Measurement System (LEMMS), part of the Magnetospheric Imaging Instrument (MIMI), *Rymer et al.* [2009] identified four different regions according to the characteristic thermal electron environment. These regions are plasma sheet (high energy and density), lobe-like (high energy,

65 low density), magnetosheath (low energy and high density) and bimodal (two superim-
66 posed populations). This classification was extended by *Smith and Rymer* [2014] to
67 include all the data gathered at Titan's orbit (with and without Titan present) by the CAPS/ELS
68 instrument until it was switched off in 2012 after 83 flybys.

69 A similar classification was made using ion data for the first 54 flybys from the
70 CAPS/IMS instrument by *Németh et al.* [2011]. They also looked at ion composition, find-
71 ing short events with enhanced heavy ion densities occurring when Cassini crossed the
72 narrow central sheet [*Németh et al.*, 2011].

73 Being located in the outer magnetosphere, the planetary magnetic field configura-
74 tion at Titan's orbit differs significantly from that of a dipolar configuration. Due to the
75 fast rotation of the planet and the presence of heavy ions, the centrifugal force causes the
76 partially corotating plasma to be confined near the equatorial regions, creating a current
77 sheet that is present at all local times, although with varying thickness [*Krimigis et al.*,
78 2007]. All of this means that the magnetic field can also be used to estimate the location
79 of Titan with respect to the magnetic equator. Using data from the Magnetometer (MAG)
80 instrument, *Simon et al.* [2010] classified the magnetic environment during the TA to T62
81 flybys. The classification was later extended to include the data until the T85 flyby [*Simon*
82 *et al.*, 2013].

83 More recently, *Kabanovic et al.* [2017] provided an empirical model of the mag-
84 netic environment at the moon's orbit using magnetic field data obtained by Cassini. They
85 found a perturbed field configuration close to noon local time, regardless of the season,
86 while a dependence on the season is present in the nightside due to the change in the ori-
87 entation of bowl-shaped current sheet.

88 The energetic plasma environment, specifically protons with energies from 27 to 255
89 keV, was studied by *Garnier et al.* [2010] for all the flybys and orbit crossings from Saturn
90 Orbit Insertion (SOI) until January 2008, almost at the end of Cassini's Prime Mission.
91 The then-total number of crossings accounted for 39 dedicated flybys and 33 crossings far
92 from Titan. In their work, they analyzed data from the MIMI suite, concentrating on the
93 LEMMS and the Ion Neutral Camera (INCA) instruments. For the former, they looked
94 at the energetic proton data (with energies between 27 and 255 keV) far from the region
95 where the disturbances introduced by Titan are appreciable. By looking at mean fluxes for
96 the channels analyzed and studying their correlation with Saturn local time (SLT), they
97 found larger fluxes in the post-midnight to dawn side.

98 It is evident from the descriptions provided above that classification of Titan's up-
99 stream environment is the least developed in terms of energetic charged particles. The
100 study of *Garnier et al.* [2010] provides some insights, but covers only a small time period
101 and is limited in energy coverage. It provides no detailed information about the shape and
102 intensity of energetic ion spectra. With the other classifications in mind (by the CAPS and
103 MAG instruments) and with the Cassini mission completed, we have the opportunity to
104 update and extend the results of *Garnier et al.* [2010] providing a more detailed descrip-
105 tion of Titan's energetic particle environment. The availability of an empirical model of
106 energetic particles is necessary to complement the study of how Titan interacts with the
107 magnetospheric environment and how the energy deposition into the atmosphere changes
108 with upstream conditions.

109 Cassini performed the first dedicated flyby of Titan on October 26, 2004. During
110 this flyby, known as the TA flyby, Cassini traveled, with an altitude at closest approach
111 (CA) of 1174km, below the main ionospheric peak, located at around 1200 km. *Cravens*
112 *et al.* [2005] compared the results obtained by the Radio and Plasma Wave Science instru-
113 ment (RPWS) during this flyby with those obtained using a photochemical model along
114 the track of the spacecraft. They showed that by just considering photoionization (without
115 the inclusion of electron impact ionization), the production rate predicted by the model

116 was significantly lower than what the data showed, making it necessary to consider the
117 magnetospheric input as well.

118 *Edberg et al.* [2015] looked at the electron densities in Titan's ionosphere at different
119 local times. After filtering out the ionization by solar EUV using a photochemical model,
120 they found higher densities during flybys that occurred around the midnight sector of the
121 magnetosphere and lower densities around noon. They suggested that this difference could
122 be due to ionization from magnetospheric sources.

123 Using data obtained by the MIMI/LEMMS instrument during the T5 flyby, *Cravens*
124 *et al.* [2008] calculated production rates from precipitating H^+ and O^+ from the magne-
125 tosphere of Saturn. They found that these ions can contribute to the ionization of the
126 atmosphere at altitudes between 500 km and 1000 km, below the main ionospheric peak
127 which is mainly produced by solar EUV radiation, a result confirmed through test particle
128 simulations by *Regoli et al.* [2016].

129 *Gronoff et al.* [2009] also analyzed the role of energetic electrons in the ionization
130 of Titan's atmosphere during the T5 flyby and concluded that the geometry of the draped
131 field lines has a significant influence on the local electron fluxes. Similar results were ob-
132 tained by *Smith et al.* [2009] by looking at energetic neutral atom (ENA) emissions pro-
133 duced by precipitating protons and detected by the MIMI/INCA instrument.

134 In terms of neutral particles, *Brandt et al.* [2012] studied the exosphere of Titan us-
135 ing energetic neutral atom (ENA) measurements from the INCA instrument. They found
136 an H_2 exosphere that extends to about 50,000 km and also estimated the precipitation of
137 ENAs to be comparable to that of energetic ions. This led to the suggestion that, for any
138 study analyzing the energy budget at Titan's atmosphere, ENAs need to be accounted for.

139 In this work we analyze the energetic environment at Titan's orbit, with a focus on
140 energetic protons. Using data from the LEMMS and CHEMS instrument, we develop a
141 method to characterize the proton fluxes and distribution encountered at Titan's orbit at
142 different locations in the magnetosphere, as well as an empirical model of the energetic
143 proton environment. The results of the present work are particularly interesting for the
144 ionization of Titan's atmosphere and for understanding ENA emissions from Titan's exo-
145 sphere, as observed by Cassini's INCA detector.

146 2 Instrumentation and dataset

147 Cassini had a series of instruments devoted to the study of charged particles at dif-
148 ferent energy levels. Among those, the Cassini Plasma Spectrometer (CAPS) and the
149 Magnetospheric Imaging Instrument (MIMI) were designed to perform in-situ measure-
150 ments of the fluxes of charged particles with different energies in Saturn's magnetosphere.

151 CAPS [*Young et al.*, 2004] was composed of three instruments, namely the Electron
152 Spectrometer (ELS), the Ion Mass Spectrometer (IMS) and the Ion Beam Spectrometer
153 (IBS). Among the three of them, ELS and IMS are of special interest when it comes to
154 characterizing the low energy environment of the Saturnian magnetosphere. ELS was used
155 to characterize the plasma environment at which Titan was encountered at each of the fly-
156 bys for which CAPS data are available [*Rymer et al.*, 2009]. Due to an electrical failure of
157 the spacecraft, CAPS was switched off shortly after the T83 flyby that took place in May
158 2012.

159 CAPS covered the low-energy part of the spectrum, with ELS reaching energies of
160 up to 28 keV and IMS reaching energies of up to 50 keV. This was neatly complemented
161 by MIMI [*Krimigis et al.*, 2004], composed by the Low Energy Magnetospheric Measure-
162 ment System (LEMMS), the Charge Energy Spectrogram (CHEMS) and the Ion and Neu-
163 tral Camera (INCA).

The data used in the present study were collected by the LEMMS and CHEMS instruments. LEMMS was mounted on a rotating platform intended to provide 360° coverage on the spacecraft's x-z plane. The platform, however, stopped working at the beginning of 2005, leaving the instrument looking into a fixed direction [Krupp *et al.*, 2012]. This limited the pitch angle coverage of the instrument, although at Titan's orbit, as reported by Garnier *et al.* [2010], the ion distribution is quasi-isotropic.

LEMMS consisted of a double-ended telescope. The two ends of the instrument measured different energy ranges, one being labeled as 'low energy' and one as 'high energy'. The low energy end was able to measure ions with energies between 27 keV and 4 MeV and electrons from 18 to 832 keV while the high energy end could measure ions with energies from 1.4 to 160 MeV/N and electrons from 0.1 to several tens of MeV [Krupp *et al.*, 2009].

For this study, only ion data gathered by the low energy telescope are used. The corresponding channels on the LEMMS instrument are labeled A0 to A7 and the energy range for each one of these channels is presented in Table 1. For most of the time when Cassini was in the outer magnetosphere near Titan's orbit, the highest-energy channels of the instrument do not measure any fluxes above the detection threshold. For this reason, some of the analyses presented here will focus on the lowest-energy channels.

Ion channel	Energy range (keV)
A0	27 - 35
A1	35 - 56
A2	56 - 106
A3	106 - 255
A4	255 - 506
A5	506 - 805
A6	805 - 1600
A7	1615 - 4000

Table 1. Energy ranges covered by individual channels of the MIMI/LEMMS instrument, adapted from Krupp *et al.* [2009].

CHEMS was a mass spectrometer capable of distinguishing between ion species and their charge state, most importantly H^+ and W^+ ions, the two major magnetospheric species present at Titan's orbit [e.g. Sergis *et al.*, 2007; Dialynas *et al.*, 2009; Thomsen *et al.*, 2010; Arridge *et al.*, 2011]. The instrument was composed of three telescopes, each one containing an electrostatic analyzer to filter particles based on their energy/charge followed by a time-of-flight (TOF) analysis to determine the mass of the detected ion. The central telescope was fairly well-aligned with the low-energy telescope of LEMMS. In terms of energies, CHEMS covered the range between 2.8 keV to 220 keV.

For all the analyses presented in the following sections of the paper, data collected between SOI and the beginning of 2017 are used. Since the focus of the paper is on the energetic H^+ environment at Titan's orbit, the data are filtered to cover the L-shell range between 19 and 21 R_S and the latitude is also limited by only including data collected within 1 R_S of the equatorial plane. In general, higher latitudes can be considered (from where fluxes can be mapped to Titan's orbital plane) but, due to the ambiguity of magnetic field models for Saturn's magnetosphere at Titan's distance, we restrict our study near the equatorial plane. For some of the analyses, subsets of the described dataset are used, as indicated at the beginning of the corresponding section.

201 When analyzing data collected during dedicated flybys, the interaction region (de-
202 fined as the region of the magnetosphere affected by the presence of the moon) is removed
203 from the data to ensure that only the magnetospheric environment is taken into account.

204 In terms of accumulation time, two different sets were used for the study. When an-
205 analyzing fluxes (sections 3 to 5), 10-minute averaged data were used, while for the Kappa
206 distribution analysis (section 6) 30-minute averaged data were used. These accumulation
207 times provide enough smoothing of the data while still capturing the possible spatial vari-
208 ations.

209 Taking into account the spatial constraints just mentioned, it took about 4 hours for
210 Cassini to fly through the region of interest. This translates into approximately 24 data
211 points available for each of the flybys and orbit crossings for the analysis for fluxes and
212 about 8 spectra for the Kappa distribution fits.

213 **3 Dependence of the energetic ion fluxes on the local plasma environment**

214 In order to correctly interpret any results involving the fluxes of energetic ions, it
215 is important to determine whether these fluxes are affected in any way by the location in
216 the magnetosphere at which Cassini was at the time the data were obtained (as is the case
217 for low energy ions and electrons). For this, the classification introduced by *Rymer et al.*
218 [2009] is used, where 6 different categories were defined, namely plasma sheet (hereafter
219 referred to as category 1), lobe-like (2), magnetosheath (3), bimodal (4), mixed (5) and
220 unclassified (6). On December 1st, 2013, Titan was encountered by Cassini while in the
221 unshocked solar wind [*Bertucci et al.*, 2015] so an extra category, namely solar wind (7),
222 will be included as well.

223 The first three categories are, as their names imply, related to the specific locations
224 inside Saturn's magnetosphere. Bimodal spectra contain two different electron populations
225 which were linked by *Rymer et al.* [2009] to an enhanced pick-up ion environment. Mixed
226 means that Cassini crossed more than one environment during the flyby or pass. Finally,
227 unclassified means that the observed spectrum does not fit in any of the first four cate-
228 gories, but at the same time it is not uniform enough as to justify the creation of a new
229 category.

230 Here we look at the ion channel with the lowest energies from LEMMS (namely A0,
231 with energies from 27 to 35 keV) in order to determine whether a correlation exists be-
232 tween the observed average fluxes and the category in which each of the flybys occurred.
233 We only use the lowest-energy channel since we are interested here in global trends in the
234 magnetosphere. An analysis containing the full distribution of high-energy particles is pre-
235 sented in Section 6.

236 The top panel of Figure 1 shows a plot of the median fluxes of the data from the
237 A0 channel obtained during each of the first 83 flybys plus T85 and T96, and a subset
238 of the orbit crossings for which the environment classification has been published [*Smith*
239 *and Rymer*, 2014]. Apart from all the flybys and orbit crossings with classification from
240 the CAPS instrument, T85 is included because it was another magnetosheath flyby [*Ed-*
241 *berg et al.*, 2013] and T96 because it was the only solar wind flyby recorded by Cassini
242 [*Bertucci et al.*, 2015]. The bottom panel shows the number of data points available at
243 each environment.

244 Table 2 shows the median values plotted in Figure 1 together with the number of
245 data points available for each case. The data points correspond to all the spectra collected
246 for the analysis and not to individual events.

252 Without taking into account the mixed and unclassified data points, from the median
253 fluxes presented in Figure 1 and Table 2, it can be seen that the A0 channel fluxes are in-

`./figures/fluxvsclass_new.jpg`

244 **Figure 1.** Median of ion fluxes from the A0 channel (27 - 35 keV) collected during the first 83 flybys plus
 245 T85 and T96, organized by plasma environment (top panel) with the error bars representing the median of the
 246 standard deviation of the measurements. Number of data points for each environment (bottom panel).

Classification	A0 flux (median)	Number of data points
Plasma sheet	115.97	1236
Lobe-like	56.96	731
Magnetosheath	68.69	135
Bimodal	26.80	192
Mixed	167.01	418
Unclassified	57.58	393
Solar wind	371.16	24

250 **Table 2.** Median of fluxes detected by the LEMMS A0 channel (in $cm^{-2}sr^{-1}keV^{-1}s^{-1}$) and number of
 251 available data points.

254 deed influenced by the moon's location, with the solar wind fluxes being the most strongly
 255 influenced followed by the plasma sheet ones. Since there is only one flyby occurring in
 256 the solar wind, the statistical significance of this result cannot be asserted, although the
 257 fact that the magnetopause and the bow shock boundaries were pushed beyond the orbit of
 258 Titan directly implies large solar wind fluxes.

259 In contrast to what is observed in the thermal plasma data from the CAPS instru-
 260 ment, the fluxes in the magnetosheath are lower than those encountered in the plasma
 261 sheet. At the same time, they are slightly higher than those in the lobes, although an im-
 262 portant overlap between both classifications exists. From the number of available data
 263 points, it is also evident that the quality of the statistics from different environments is
 264 different, with the plasma sheet and the lobe regions inside the magnetosphere being the
 265 better sampled.

266 Another way of looking at the data whilst considering all the data points available is
 267 to make a rough distinction between plasma sheet and lobes based on the magnetic field
 268 data. This can be achieved by plotting the fluxes vs. the ratio between the radial compo-
 269 nent of the magnetic field and the magnitude of the field. When this ratio is close to zero,
 270 it means the magnetic field is almost perpendicular to the orbit plane, meaning that the
 271 data were collected close to the center of the current sheet. Figure 2 shows a scatter of all
 272 the A0 channel measurements included in the study plotted against $B_r/|B|$, together with
 273 a second degree polynomial fit that shows the trend towards higher fluxes closer to the
 274 center of the current sheet, and lower fluxes at the lobes.

`./figures/a0_vs_brbmag.jpg`

275 **Figure 2.** Ion fluxes from the A0 channel of the MIMI/LEMMS instrument vs. location with respect to the
 276 center of the current sheet. The orange line shows a second order polynomial fit to the median of the data.

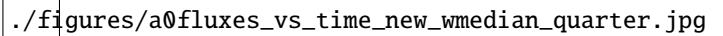
277 In general, although with some overlap between the lobe-like and magnetosheath
 278 regions, the data follows a trend that is expected, with the fluxes in the plasma sheet being

279 higher than those in the lobes. Using a single channel, though, provides an incomplete
280 description of the environment.

281 In addition to the difference in kinetic energy, the overall shape of the distribution
282 is another factor that makes it possible to use the thermal plasma data for classification
283 but not the energetic data. The *Rymer et al.* [2009] and *Németh et al.* [2011] classifications
284 rely on two main factors to define the different categories, namely flux and energy of the
285 peak of the distribution. While the fluxes can vary for energetic data as well, the peak of
286 the distribution is always located at the lowest energy channels of the MIMI instrument.

287 4 Ion fluxes over time

288 Figure 3 shows the ion fluxes detected by the A0 channel of the instrument between
289 Saturn orbit insertion (SOI) in 2004 and the beginning of 2017. The plot includes all the
290 data gathered during that period at Titan's orbit, regardless of the plasma environment or
291 local time. It also includes both flybys and orbit crossings.

./figures/a0fluxes_vs_time_new_wmedian_quarter.jpg

292 **Figure 3.** Ion fluxes from the A0 channel of the MIMI/LEMMS instrument sampled between 2004 (SOI)
293 and beginning of 2017. The orange line shows the median of the fluxes for consecutive periods of time cover-
294 ing 3 months.

295 It can be seen that no clear seasonal dependence is present and overall the fluxes
296 are highly variable. As representative of higher or lower fluxes than the general trend, five
297 specific periods are highlighted in the plot. These correspond to the times listed in Table
298 3 together with some relevant parameters.

Date	A0 flux	SLT	Flyby/Pass	Classification
2006-11-30	57.15	2.17	Pass	Lobe-like
2007-06-13	1.36×10^3	13.56	Flyby (T32)	Magnetosheath
2010-08-15	130.02	15.90	Pass	Current sheet
2011-09-12	6.15×10^3	17.69	Flyby (T78)	Current sheet
2013-12-01	4.62×10^3	12.37	Flyby (T96)	Solar wind

299 **Table 3.** Characteristics of four selected data points for ion fluxes from the A0 channel (fluxes in
300 $cm^{-2}sr^{-1}keV^{-1}s^{-1}$).

301 The three highlighted time periods with high fluxes coincide with two dedicated fly-
302 bys, namely T32, T78 and T96. T32 was the first flyby of the mission that occurred with
303 Titan inside the magnetosheath. The fact that Titan was located outside the magnetosphere
304 means that the solar wind was energized and, even after being slowed down past the bow
305 shock, the distribution of ions detected by Cassini was energized enough that the LEMMS
306 instrument was able to capture an enhanced flux of particles.

307 The case of T78 is quite different. While T32 occurred at the noon sector of the
308 magnetosphere, specifically at 13.56 SLT, T78 occurred in the afternoon sector, at 17.55
309 SLT. Furthermore, the flyby was classified using MAG data by *Simon et al.* [2013] as
310 having taken place under plasma sheet conditions. At the time of the flyby, CAPS was

311 switched off, so no classification from the low-energy plasma point of view is available
312 [*Smith and Rymer, 2014*].

313 The third highlighted point corresponds to the T96 flyby, that took place at a time
314 when the magnetosphere was compressed by the arrival of an ICME and it corresponds to
315 the only flyby during the Cassini mission when Titan was observed in the solar wind.

316 High fluxes are also visible for the very first dataset which corresponds to the TA
317 flyby. Being the first flyby of the mission, TA was studied in detail using different data
318 sets and simulations and it was found that the fluxes were relatively high, comparable to
319 those observed by Voyager 1 [e.g. *Backes et al., 2005; Cravens et al., 2005; Hartle et al.,*
320 *2006*].

321 For the case of low fluxes, two times are highlighted in Figure 3. Both of them cor-
322 respond to crossings of Titan’s orbit, with the first datapoint having been collected at 2.16
323 SLT and the second one at 15.9 SLT. The selection of these datapoints was solely based
324 on their relatively low fluxes as shown in Figure 3 and, at first glance, no noticeable fea-
325 tures that could explain the low fluxes are present.

326 Given their lack of interaction with the solar wind boundaries, solar energetic parti-
327 cles (SEP) can penetrate the magnetosphere and thus serve as a proxy for the solar wind
328 activity when Cassini was inside the magnetosphere of Saturn. A series of these events
329 was identified by *Roussos et al. [2017]*. The data points for the A0 and A5 channels that
330 fall within the period of time when these SEP events were detected are highlighted in or-
331 ange in Figure 4.

./figures/septimes.jpg

332 **Figure 4.** Ion fluxes from the A0 (top) and A5 (bottom) channels of MIMI/LEMMS showing periods when
333 SEP events were observed at Saturn highlighted in orange.

334 In general, although SEP events increase the fluxes in the highest energy channels of
335 the LEMMS instrument [*Roussos et al., 2017*], the effect does not seem to be as strong in
336 the lowest energy channels. This is not completely unexpected, given that the ability of a
337 particle to penetrate the bow shock depends on the particle’s energy, and those detected by
338 the A0 channel might simply not have the energy needed to do so. This is apparent when
339 comparing the fluxes of the SEP events in both channels shown in Figure 4. While those
340 from the A0 channel show no special trend, the ones detected by the A5 channel do have
341 a bias towards higher fluxes.

342 5 Average fluxes

343 In this section, the local time dependence of the energetic ion fluxes is analyzed. For
344 this, all the data available from the lowest energy ion channel (A0) between SOI and the
345 beginning of 2017 are taken into account.

346 Figure 5 shows a plot of the median ion fluxes vs. SLT divided into two-hour bins
347 for the two main magnetospheric environments, namely current sheet (top) and lobe-like
348 (bottom). Since the data are being divided by magnetospheric environment, only those
349 times listed in *Rymer et al. [2009]* and *Smith and Rymer [2014]* are used. Both plots show
350 the number of data points available at each SLT bin. The sampling is rather low for most
351 bins and, for some of them there are no points available at all. The dayside/nightside
352 asymmetry reported by *Garnier et al. [2010]* is not observable, although their analysis did
353 not discern between magnetospheric environments.

`./figures/slt_class_errorbars_new.jpg`

354 **Figure 5.** Median of ion fluxes from the A0 channel at two different magnetospheric environments, namely
 355 current sheet (top panel) and lobe-like (bottom panel). The error bars correspond to the standard error of the
 356 medians. The right axes of the plots show the number of data points available at each SLT bin.

357 When the environment restriction is removed, the plot shown in Figure 6 is ob-
 358 tained. In this plot an SLT asymmetry seems to be present, with the largest fluxes present
 359 between the afternoon and pre-midnight sector of the magnetosphere. However, the sam-
 360 pling bias observed in Figure 5 shows that many of the measurements taken in the night-
 361 side (especially in the pre-midnight sector, where fluxes seem to be higher) were made
 362 when Titan was in the current sheet, a region that, as shown in Figure 1, presents larger
 363 fluxes of energetic particles.

`./figures/a0_vs_slt_new.jpg`

364 **Figure 6.** Median of ion fluxes from the A0 channel. The error bars correspond to the standard error of the
 365 medians and the orange curve shows a sinusoidal fit to the data.

366 Part of the asymmetry in SLT observed in the electron densities in the ionosphere,
 367 as reported by *Edberg et al.* [2015] can be due to this sampling bias. While energetic par-
 368 ticles are expected to penetrate below the altitude of Cassini’s closest approach [*Cravens*
 369 *et al.*, 2008; *Regoli et al.*, 2016], part of the incident population could have grazing angles
 370 large enough that they will indeed deposit their energy at higher altitudes.

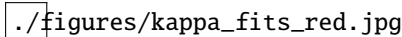
371 6 Analysis of energetic H^+ spectra using Kappa distributions

372 Kappa distributions were first introduced by *Vasyliunas* [1968] to describe the spec-
 373 tra of plasma populations that could not be described with Maxwellian distributions in
 374 the Earth’s magnetosphere and have since then been used to describe populations in other
 375 planetary magnetospheres [*Dialynas et al.*, 2017] and plasma environments [e.g. *Livadi-*
 376 *otis and McComas*, 2013; *Livadiotis*, 2015]. In this study we use a simplified version of
 377 the original distribution that was described in *Dialynas et al.* [2009], based on a function
 378 introduced by *Mauk et al.* [2004] for the study of energetic ions in the Jovian magneto-
 379 sphere.

380 Due to the energy distribution of particles in the magnetosphere, the MIMI/LEMMS
 381 and MIMI/CHEMS instruments capture the high-energy tail of a Kappa distribution cen-
 382 tered at low energies that is detected by the CAPS instrument [*Young et al.*, 2005; *Dia-*
 383 *lynas et al.*, 2009]. The high energy fluxes have been organized by the value of the pa-
 384 rameters of a Kappa distribution for the equatorial magnetosphere of Saturn, but no spe-
 385 cific analysis for Titan’s orbit has been made thus far, apart from the fact that the *Dialynas*
 386 *et al.* [2009] study included data collected by Cassini only until July 2007. In this section,
 387 a modified Kappa distribution function (Equation 1) is used with the aim of providing an
 388 empirical model of the fluxes of energetic particles at Titan’s orbit.

$$j = C \cdot E[E + kT(1 + \kappa)]^{-(1+\kappa)} \quad (1)$$

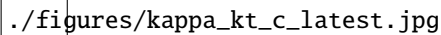
389 Figure 7 shows two examples of the combined LEMMS and CHEMS spectra used
 390 in this study for two different times, together with the corresponding result of the fitting
 391 process. As visible from both spectra shown, the Kappa distribution function provides a
 392 good description of the plasma population with energies above 20 keV, whereas below
 393 that threshold, the distribution seems to be closer to an inverse power law, which is most
 394 likely representative of a second Kappa distribution that peaks at lower energies [*Dialynas*
 395 *et al.*, 2009]. For instance, *Young et al.* [2005] showed broad peaks of ions at local corota-
 396 tion speeds. This change in the distribution is particularly visible in the right-hand panel
 397 of Figure 7 and it implies that the results presented in this section in terms of an empiri-
 398 cal model of the fluxes are only valid for energies above 20 keV.

./figures/kappa_fits_red.jpg

399 **Figure 7.** Combined LEMMS and CHEMS spectra and result of the fitting process for two different time
 400 periods. The error bars correspond to the standard deviation of the measurements.

401 Due to the already described variabilities of the outer magnetosphere, when analyz-
 402 ing the results of the fitting process the different possible sources of this variability need
 403 to be considered. These include location where the data were collected with respect to
 404 Saturn (SLT), location with respect to the current sheet (magnetic latitude) and whether
 405 the data were collected inside or outside the magnetosphere (only relevant for flybys or
 406 passes that occurred close to the subsolar point, or close to 12 SLT).

407 Figure 8 shows the results of organizing the κ , kT and C parameters with respect
 408 to Saturn local time. In the cases of κ and kT it can be seen that the values are in good
 409 agreement with what was reported by *Dialynas et al.* [2009] for the outer magnetosphere.
 410 However, no clear trend is present in any of them.

./figures/kappa_kt_c_latest.jpg

411 **Figure 8.** κ (top panel) and kT (center panel) and C (bottom panel) parameters organized by Saturn local
 412 time (SLT). The data points correspond to the median of all the values at each SLT bin and the error bars
 413 represent the standard deviation.

414 Since most plasma sources in Saturn's magnetosphere are located in the inner region
 415 (with the main source, Enceladus, at a radial distance of 4 R_S), by the time the plasma is
 416 transported outwards, any SLT asymmetries that could be originally present are smoothed
 417 out. This was shown by *Dialynas et al.* [2013] where they analyzed ion distributions from
 418 the MIMI instrument at radial distances between 5 and 20 R_S and showed that the inner
 419 magnetosphere presents significant structure (especially on the dayside) that decreases with
 420 increasing L-shell.

421 Figure 9 shows the same parameters from the fits, this time organized by plasma
 422 environment using, once again, the classification from *Rymer et al.* [2009].

426 For the four well-defined environments all the three parameters show a similar trend,
 427 with the lowest values present for solar wind conditions, followed by plasma sheet, lobe-
 428 like and magnetosheath conditions, where the maximum values are observed. There is,
 429 however, a significant spread in the data, another reflection of the variability of the ener-
 430 getic environment.



423 **Figure 9.** κ (top panel) and kT (center panel) and C (bottom panel) parameters organized by magneto-
 424 spheric environment according to *Rymer et al.* [2009] classification. The orange points correspond to the
 425 median of all the values at each SLT bin and the error bars represent the standard deviation.

431 Table 4 presents the obtained median values of the three parameters. The κ parame-
 432 ter indicates the shape of the distribution, with a larger value meaning a more thermalized
 433 population. For this reason, it is interesting to analyze the κ value obtained for each envi-
 434 ronment.

435 The classification used was obtained using thermal electron data, and thus the link
 436 to energetic ions might be weak. This makes it difficult to interpret the results obtained,
 437 especially for cases like the bimodal distribution, which is based on an extra source of
 438 thermal electrons that might not be linked at all to energetic particles. For similar rea-
 439 sons, the results for the mixed and unclassified environments are only useful in a statistical
 440 sense and a physical interpretation is difficult to be derived.

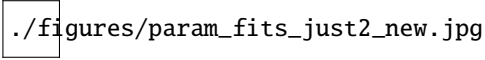
441 For the other four environments, while the link between the thermal electron data
 442 and the energetic particles might be, at best, weak, some physical interpretation can be
 443 given to the results, keeping in mind that the statistical uncertainty of the values obtained
 444 is significant when compared to the difference between the values at specific environ-
 445 ments. In general, the value of κ obtained for the solar wind is consistent with results
 446 reported in the literature (see for instance Table 1.1 in *Livadiotis* [2017]).

447 The fact that, in average, the value of κ at the magnetosheath is larger than at the
 448 plasma sheet and the lobes could be related to a thermalization of the solar wind plasma.
 449 However, the shape of the distribution will also depend on external parameters such as the
 450 Alfvén mach number and the plasma beta [e.g. *Thomsen et al.*, 2018] at any given point
 451 and these values will necessarily be smoothed by the averaging performed in the analysis
 452 presented here.

Classification	Kappa	kT	C	STD(C)
Plasma sheet	4.78	9.31	2.15×10^{12}	7.68×10^{12}
Lobe-like	4.78	7.64	2.47×10^{11}	4.99×10^{12}
Magnetosheath	5.04	5.75	1.13×10^{13}	8.12×10^{12}
Bimodal	5.43	8.37	5.74×10^{12}	3.08×10^{12}
Mixed	4.41	7.90	7.39×10^{10}	7.41×10^{12}
Unclassified	4.93	10.80	8.57×10^{12}	7.00×10^{12}
Solar wind	2.42	6.30	2.02×10^6	2.40×10^6

453 **Table 4.** Median values of the three parameters of the Kappa distribution function organized by magneto-
 454 spheric environment.

455 In order to simplify the environment description, we have also looked for correlation
 456 between the three spectrum coefficients, so that we can reduce the free parameters of the
 457 spectrum from three to one. In terms of interdependence of the parameters, the plots from
 458 Figure 10 show the κ (top panel) and kT (bottom panel) parameters plotted against C .



459 **Figure 10.** Correlation between different parameters of the Kappa distribution function (Equation 1). The
460 blue points are the values obtained from the fits while the colored curves represent different fits to the data.

461 The black points in both panels show the respective values obtained from the fits
462 described above together with the error bars that are obtained from the quality of the fits.
463 In addition, the two orange curves represent fits to the data.

464 Both plots show a power-law dependence (Equations 2 and 3 respectively), with a
465 spread present for large values of C , where most of the points are concentrated (about half
466 of the fits throw a value for C that is larger than 5×10^{12}). The goodness of the fit in terms
467 of R-square for the κ vs. C case is 0.8757 and for the kT vs. C case is 0.3672. This dif-
468 ference is already visible in Figure 10 from the larger spread of kT for low values of C .

$$\kappa = -9.915 \cdot C^{-0.03768} + 8.421 \quad (2)$$

$$kT = 0.7155 \cdot C^{0.08844} + 1.028 \quad (3)$$

469 The combination of the values of C provided for each magnetospheric environment
470 together with the relations from Equations 2 and 3 provide a description of the energetic
471 particle fluxes at different environments.

472 7 Discussion and Conclusions

473 During the time orbiting Saturn, Cassini sampled different regions of the magneto-
474 sphere gathering enough data to understand part of the dynamics of the plasma circula-
475 tion. Still, due to the size of the magnetosphere, the coverage is far from perfect. If we
476 add this to the fact of only having a single spacecraft to analyze the dynamic processes
477 that take place in the outer regions of the magnetosphere, characterizing the magneto-
478 spheric environment at Titan's orbit is a very challenging task.

479 Given that about 50% of the particle pressure in the magnetosphere of Saturn is
480 contributed by the energetic particles [Sergis *et al.*, 2009], understanding the fluxes from
481 a statistical point of view is important to provide a comprehensive model of the interac-
482 tion of Titan with the Saturnian magnetosphere. In addition, an empirical model of the
483 ion fluxes can help constrain the energy deposition by energetic particles that affect mainly
484 the ionospheric densities below the main ionospheric peak.

485 While some progress has been made with the magnetic field and low-energy particle
486 data, few studies have focused on the high-energy plasma. In this paper, we analyzed data
487 from the MIMI/LEMMS and MIMI/CHEMS instruments in order to study, from a statisti-
488 cal point of view, the behavior of energetic H^+ ions. Towards this, we looked at the mean
489 fluxes detected by LEMMS and also at the energy distribution by fitting Kappa distribu-
490 tion functions to the data.

491 Based on the analyses detailed on the paper, we conclude that the energetic envi-
492 ronment is extremely variable. As expected based on prior studies and on this one, when
493 looking at ions in the keV and MeV scale, we are only looking at the high-energy part of
494 the total particle distribution and these particles, due to their high kinetic energy, are not
495 as cleanly organized by their location with respect to the center of the plasma sheet as
496 thermal particles are.

Fluxes in the higher-energy channels are notably increased during SEP events. This increase in the fluxes can be related to acceleration processes arising from the arrival of the SEPs or to the fact that solar wind ions with very high energies can penetrate the magnetosphere, thus reaching the moon even when located downstream of the magnetopause. In both cases, this implies that the energy deposition in the atmosphere might be affected during periods of enhanced solar activity, something that needs to be further analyzed to evaluate how the ionosphere below the main peak is affected.

With the aim of providing an empirical model of the energetic particle environment, instead of looking at the fluxes of a single energy channel, a better approach is to look at the distribution of particles. At the energies analyzed in this study, we see the high energy tail of a Kappa distribution that peaks at low energies, and a Kappa distribution of an energized population, peaking at approximately 20 keV. In this sense, we derived correlations between the parameters describing this high-energy population as a Kappa distribution function.

While no local time dependence was found, there is a correlation of the Kappa distribution parameters and the magnetospheric environment and also between the different parameters of the distribution. More than half of the periods analyzed have values of C , kT and κ within specific ranges. Apart from this, there is a strong power-law correlation between κ and C and between kT and C .

Acknowledgments

This work was carried out in the frame of the International Max Planck Research School (IMPRS) for Solar System Science at the Max Planck Institute for Solar System Research (MPS) as well as at the Mullard Space Science Laboratory (UCL) and the University of Michigan (UM). The German contribution of MIMI/LEMMS was in part financed by BMBF through DLR under contract 50OH1101 and by the Max Planck Gesellschaft. L. H. Regoli has received funds from an Impact Scholarship awarded by a collaboration between the University College London (UCL) and the Max Planck Society (MPG) and by a NASA Living With a Star grant (NNX16AL12G). AJC, GHJ and IJR acknowledge support from the STFC consolidated grants to UCL-MSSL ST/K000977/1 and ST/N000722/1. Cassini data are available through NASA's planetary data system (PDS).

References

- Achilleos, N., C. S. Arridge, C. Bertucci, C. M. Jackman, M. K. Dougherty, K. K. Khurana, and C. T. Russell (2008), Large-scale dynamics of Saturn's magnetopause: Observations by Cassini, *Journal of Geophysical Research*.
- Arridge, C. S., K. K. Khurana, C. T. Russell, D. J. Southwood, N. Achilleos, M. K. Dougherty, A. J. Coates, and H. K. Leinweber (2008), Warping of Saturn's magnetospheric and magnetotail current sheets, *Journal of Geophysical Research*.
- Arridge, C. S., N. André, C. L. Bertucci, P. Garnier, C. M. Jackman, Z. Németh, A. M. Rymer, N. Sergis, K. Szego, A. J. Coates, and F. J. Crary (2011), Upstream of Saturn and Titan, *Space Science Reviews*, 162, 25–83.
- Backes, H., F. M. Neubauer, M. K. Dougherty, N. Achilleos, N. André, C. S. Arridge, C. Bertucci, G. H. Jones, K. K. Khurana, C. T. Russell, and A. Wennmacher (2005), Titan's Magnetic Field Signature During the First Cassini Encounter, *Science*.
- Bertucci, C., N. Achilleos, M. K. Dougherty, R. Modolo, A. J. Coates, K. Szego, A. Masters, Y. Ma, F. M. Neubauer, P. Garnier, J.-E. Wahlund, and D. T. Young (2008), The Magnetic Memory of Titan's Ionized Atmosphere, *Science*.
- Bertucci, C., D. C. Hamilton, W. S. Kurth, G. Hospodarsky, D. Mitchell, N. Sergis, N. J. T. Edberg, and M. K. Dougherty (2015), Titan's interaction with the supersonic solar wind, *Geophysical Research Letters*.

- 546 Brain, D. A., D. Hurley, and M. R. Combi (2010), The solar wind interaction
547 with Mars: Recent progress and future directions, *Icarus*, 206(1), 1–4, doi:
548 10.1016/j.icarus.2009.10.020.
- 549 Brandt, P. C., K. Dialynas, I. Dandouras, D. G. Mitchell, P. Garnier, and S. M. Krimigis
550 (2012), The distribution of Titan’s high-altitude (out to ~50,000 km) exosphere from
551 energetic neutral atom (ENA) measurements by Cassini/INCA, *Planetary and Space Sci-*
552 *ence*, 60(1), 107–114, doi:10.1016/j.pss.2011.04.014.
- 553 Brecht, S. H., and S. A. Ledvina (2006), The Solar Wind Interaction With the Martian
554 Ionosphere/Atmosphere, *Space Science Reviews*, 126, 15–38, doi:10.1007/s11214-006-
555 9084-z.
- 556 Cravens, T. E., I. P. Robertson, J. Clark, J.-E. Wahlund, J. H. W. Jr., S. A. Ledvina,
557 H. B. Niemann, R. V. Yelle, W. T. Kasprzak, J. G. Luhmann, R. L. McNutt, W.-H. Ip,
558 V. D. L. Haye, I. Müller-Wodarg, D. T. Young, and A. J. Coates (2005), Titan’s iono-
559 sphere: Model comparisons with Cassini Ta data, *Geophysical Research Letters*, 32(12).
- 560 Cravens, T. E., I. P. Robertson, S. A. Ledvina, D. Mitchell, S. M. Krimigis, and J. H.
561 Waite (2008), Energetic ion precipitation at Titan, *Geophysical Research Letters*, 35,
562 doi:10.1029/2007GL032451.
- 563 Dialynas, K., S. M. Krimigis, D. G. Mitchell, D. C. Hamilton, N. Krupp, and P. C. Brandt
564 (2009), Energetic ion spectral characteristics in the Saturnian magnetosphere using
565 Cassini/MIMI measurements, *Journal of Geophysical Research*.
- 566 Dialynas, K., P. C. Brandt, S. M. Krimigis, D. G. Mitchell, D. C. Hamilton, N. Krupp,
567 and A. M. Rymer (2013), The extended Saturnian neutral cloud as revealed by global
568 ENA simulations using Cassini/MIMI measurements, *Journal of Geophysical Research*
569 (*Space Physics*), 118, 3027–3041, doi:10.1002/jgra.50295.
- 570 Dialynas, K., C. P. Paranicas, J. F. Carbary, M. Kane, S. M. Krimigis, and B. H. Mauk
571 (2017), The Kappa-Shaped Particle Spectra in Planetary Magnetospheres, in *Kappa Dis-*
572 *tributions*, chap. 12, pp. 481–522, Elsevier.
- 573 Edberg, N. J. T., D. J. Andrews, O. Shebanits, K. Ågren, J.-E. Wahlund, H. J. Opgenoorth,
574 E. Roussos, P. Garnier, T. E. Cravens, S. V. Badman, R. Modolo, C. Bertucci, and
575 M. K. Dougherty (2013), Extreme densities in Titan’s ionosphere during the T85 mag-
576 netosheath encounter, *Geophysical Research Letters*.
- 577 Edberg, N. J. T., D. J. Andrews, C. Bertucci, D. A. Gurnett, M. K. G. Holmberg,
578 C. M. Jackman, W. S. Kurth, J. D. Menietti, H. J. Opgenoorth, O. Shebanits, E. Vi-
579 gren, and J.-E. Wahlund (2015), Effects of Saturn’s magnetospheric dynamics on
580 Titan’s ionosphere, *Journal of Geophysical Research*, 120(10), 8884–8898, doi:
581 10.1002/2015JA021373.
- 582 Garnier, P., I. Dandouras, D. Toublanc, E. C. Roelof, P. C. Brandt, D. G. Mitchell, S. M.
583 Krimigis, N. Krupp, D. C. Hamilton, and J.-E. Wahlund (2010), Statistical analysis of
584 the energetic ion and ENA data for the Titan environment, *Planetary and Space Science*.
- 585 Gronoff, G., J. Lilensten, and R. Modolo (2009), Ionization processes in the atmosphere
586 of Titan II. Electron precipitation along magnetic field lines, *Astronomy & Astrophysics*,
587 506, 965–970, doi:10.1051/0004-6361-200912125.
- 588 Hartle, R. E., E. C. Sittler, F. M. Neubauer, R. E. Johnson, H. T. Smith, F. Crary, D. J.
589 McComas, D. T. Young, A. J. Coates, D. Simpson, S. Bolton, D. Reisenfeld, K. Szego,
590 J. J. Berthelier, A. Rymer, J. Vilppola, J. T. Steinberg, and N. Andre (2006), Prelim-
591 inary interpretation of Titan plasma interaction as observed by the Cassini Plasma
592 Spectrometer: Comparisons with Voyager 1, *Geophysical Research Letters*, 33, doi:
593 10.1029/2005GL024817.
- 594 Kabanovic, S., S. Simon, F. M. Neubauer, and Z. Meeks (2017), An Empirical
595 Model of Titan’s Magnetic Environment During the Cassini Era: Evidence for Sea-
596 sonal Variability, *Journal of Geophysical Research (Space Physics)*, 122, 11, doi:
597 10.1002/2017JA024402.
- 598 Krimigis, S. M., D. G. Mitchell, D. C. Hamilton, S. Livi, J. Dandouras, S. Jaskulek, T. P.
599 Armstrong, J. D. Boldt, A. F. Cheng, G. Gloeckler, J. R. Hayes, K. C. Hsieh, W.-H.

- 600 Ip, E. P. Keath, E. Kirsch, N. Krupp, L. J. Lanzerotti, R. Lundgren, B. H. Mauk, R. W.
601 McEntire, E. C. Roelof, C. E. Schlemm, B. E. Tossman, B. Wilken, and D. J. Williams
602 (2004), Magnetosphere Imaging Instrument (MIMI) on the Cassini Mission to Sat-
603 urn/Titan, *Space Science Reviews*, *114*, 233–329, doi:10.1007/s11214-004-1410-8.
- 604 Krimigis, S. M., N. Sergis, D. G. Mitchell, D. C. Hamilton, and N. Krupp (2007),
605 A dynamic, rotating ring current around Saturn, *Nature*, *450*, 1050–1053, doi:
606 10.1038/nature06425.
- 607 Krupp, N., E. Roussos, A. Lagg, J. Woch, A. L. Müller, S. M. Krimigis, D. G. Mitchell,
608 E. C. Roelof, C. Paranicas, J. Carbary, G. H. Jones, D. C. Hamilton, S. Livi, T. P. Arm-
609 strong, M. K. Dougherty, and N. Sergis (2009), Energetic particles in Saturn’s magneto-
610 sphere during the Cassini nominal mission (July 2004 - July 2008), *Planetary and Space*
611 *Science*, *57*(14-15), 1754–1768, doi:10.1016/j.pss.2009.06.010.
- 612 Krupp, N., E. Roussos, P. Kollmann, C. Paranicas, D. G. Mitchell, S. M. Krimigis,
613 A. Rymer, G. H. Jones, C. S. Arridge, T. P. Armstrong, and K. K. Khurana (2012),
614 The Cassini Enceladus encounters 2005–2010 in the view of energetic electron mea-
615 surements, *Icarus*, *218*(1), 433–447, doi:10.1016/j.icarus.2011.12.018.
- 616 Livadiotis, G. (2015), Introduction to special section on Origins and Properties of Kappa
617 Distributions: Statistical Background and Properties of Kappa Distributions in Space
618 Plasmas, *Journal of Geophysical Research*, *120*(3), 1607–1619.
- 619 Livadiotis, G. (2017), Chapter 1 - statistical background of kappa distributions: Connec-
620 tion with nonextensive statistical mechanics, in *Kappa Distributions*, edited by G. Liva-
621 diotis, pp. 3 – 63, Elsevier, doi:https://doi.org/10.1016/B978-0-12-804638-8.00001-2.
- 622 Livadiotis, G., and D. J. McComas (2013), Understanding Kappa Distributions: A Toolbox
623 for Space Science and Astrophysics, *Space Science Reviews*, *175*(1), 183–214.
- 624 Mauk, B. H., D. G. Mitchell, R. W. McEntire, C. P. Paranicas, E. C. Roelof, D. J.
625 Williams, S. M. Krimigis, and A. Lagg (2004), Energetic ion characteristics and neutral
626 gas interactions in Jupiter’s magnetosphere, *Journal of Geophysical Research*, *109*(A9).
- 627 Németh, Z., K. Szego, Z. Bebesi, G. Erdős, L. Foldy, A. Rymer, E. C. Sittler, A. J.
628 Coates, and A. Wellbrock (2011), Ion distributions of different Kronian plasma regions,
629 *Journal of Geophysical Research*, *116*(A9), doi:10.1029/2011JA016585.
- 630 Neubauer, F. M., D. A. Gurnett, J. D. Scudder, and R. E. Hartle (1984), Titan’s magneto-
631 spheric interaction, in *Saturn*, edited by T. Gehrels and M. S. Matthews, University of
632 Arizona Press.
- 633 Regoli, L. H., E. Roussos, M. Feyerabend, G. H. Jones, N. Krupp, A. J. Coates, S. Simon,
634 U. Motschmann, and M. K. Dougherty (2016), Access of energetic particles to Titan’s
635 exobase: A study of Cassini’s T9 flyby, *Planetary and Space Science*, *130*, 40–53, doi:
636 10.1016/j.pss.2015.11.013.
- 637 Roussos, E., C. M. Jackman, M. F. Thomsen, W. S. Kurth, S. V. Badman, C. Paranicas,
638 P. Kollmann, N. Krupp, R. Bucik, D. G. Mitchell, S. M. Krimigis, D. C. Hamilton, and
639 A. Radioti (2017), Solar Energetic Particles (SEP) and Galactic Cosmic Rays (GCR) as
640 tracers of solar wind conditions near Saturn: event lists and applications, *Icarus*, doi:
641 10.1016/j.icarus.2017.08.040.
- 642 Russell, C. T., J. G. Luhmann, and R. J. Strangeway (2006), The solar wind interaction
643 with Venus through the eyes of the Pioneer Venus Orbiter, *Planetary and Space Science*,
644 *54*, 1482–1495, doi:10.1016/j.pss.2006.04.025.
- 645 Rymer, A. M., H. T. Smith, A. Wellbrock, A. J. Coates, and D. T. Young (2009), Discrete
646 classification and electron energy spectra of Titan’s varied magnetospheric environment,
647 *Geophysical Research Letters*, *36*, doi:10.1029/2009GL039427.
- 648 Sergis, N., S. M. Krimigis, D. G. Mitchell, D. C. Hamilton, N. Krupp, B. M. Mauk, E. C.
649 Roelof, and M. Dougherty (2007), Ring current at Saturn: Energetic particle pressure in
650 Saturn’s equatorial magnetosphere measured with Cassini/MIMI, *Geophysical Research*
651 *Letters*, *34*(9), doi:10.1029/2006GL029223.
- 652 Sergis, N., S. M. Krimigis, D. G. Mitchell, D. C. Hamilton, N. Krupp, B. H. Mauk, E. C.
653 Roelof, and M. K. Dougherty (2009), Energetic particle pressure in Saturn’s magneto-

- 654 sphere measured with the Magnetospheric Imaging Instrument on Cassini, *Journal of*
 655 *Geophysical Research (Space Physics)*, 114, A02214, doi:10.1029/2008JA013774.
- 656 Simon, S., A. Wennmacher, F. M. Neubauer, C. L. Bertucci, H. Kriegel, J. Saur, C. T.
 657 Russell, and M. K. Dougherty (2010), Titan's highly dynamic magnetic environment: A
 658 systematic survey of Cassini magnetometer observations from flybys TA-T62, *Planetary*
 659 *and Space Science*, 58(10), 1230–1251, doi:10.1016/j.pss.2010.04.021.
- 660 Simon, S., S. C. van Treeck, A. Wennmacher, J. Saur, F. M. Neubauer, C. L. Bertucci,
 661 and M. K. Dougherty (2013), Structure of Titan's induced magnetosphere under varying
 662 background magnetic field conditions: Survey of Cassini magnetometer data from flybys
 663 TA-T85, *Journal of Geophysical Research*, 118(4), 1679–1699, doi:10.1002/jgra.50096.
- 664 Slavin, J. A., R. C. Elphic, C. T. Russell, F. L. Scarf, J. H. Wolfe, J. D. Mihalov, D. S.
 665 Intriligator, L. H. Brace, H. A. Taylor, and R. E. Daniell (1980), The solar wind inter-
 666 action with Venus - Pioneer Venus observations of bow shock location and structure,
 667 *Journal of Geophysical Research*, 85, 7625–7641, doi:10.1029/JA085iA13p07625.
- 668 Smith, H. T., and A. M. Rymer (2014), An empirical model for the plasma environment
 669 along Titan's orbit based on Cassini plasma observations, *Journal of Geophysical Re-*
 670 *search*, 119(7), 5674–5684, doi:10.1002/2014JA019872.
- 671 Smith, H. T., D. G. Mitchell, R. E. Johnson, and C. P. Paranicas (2009), Investigation of
 672 energetic proton penetration in Titan's atmosphere using the Cassini INCA instrument,
 673 *Planetary and Space Science*, 57(13), 1538–1546, doi:10.1016/j.pss.2009.03.013.
- 674 Thomsen, M. F., D. B. Reisenfeld, D. M. Delapp, R. L. Tokar, D. T. Young, F. J. Crary,
 675 E. C. Sittler, M. A. McGraw, and J. D. Williams (2010), Survey of ion plasma pa-
 676 rameters in Saturn's magnetosphere, *Journal of Geophysical Research*, 115(A10), doi:
 677 10.1029/2010JA015267.
- 678 Thomsen, M. F., A. J. Coates, C. M. Jackman, N. Sergis, X. Jia, and K. C. Hansen
 679 (2018), Survey of magnetosheath plasma properties at saturn and inference of upstream
 680 flow conditions, *Journal of Geophysical Research: Space Physics*, 123(3), 2034–2053,
 681 doi:10.1002/2018JA025214.
- 682 Vasyliunas, V. M. (1968), A survey of low-energy electrons in the evening sector of the
 683 magnetosphere with OGO 1 and OGO 3, *Journal of Geophysical Research*, 73, 2839–
 684 2884, doi:10.1029/JA073i009p02839.
- 685 Wei, H. Y., C. T. Russell, M. K. Dougherty, F. M. Neubauer, and Y. J. Ma (2010), Upper
 686 limits on Titan's magnetic moment and implications for its interior, *Journal of Geophys-*
 687 *ical Research*.
- 688 Young, D. T., J. J. Berthelier, M. Blanc, J. L. Burch, A. J. Coates, R. Goldstein,
 689 M. Grande, T. W. Hill, R. E. Johnson, V. Kelha, D. J. McComas, E. C. Sittler, K. R.
 690 Svenes, K. Szegö, P. Tanskanen, K. Ahola, D. Anderson, S. Bakshi, R. A. Baragi-
 691 ola, B. L. B. R. K. Black, S. Bolton, T. Booker, R. Bowman, P. Casey, F. J. Crary,
 692 D. Delapp, G. Dirks, N. Eaker, H. Funsten, J. D. Furman, J. T. Gosling, H. Hannula,
 693 C. Holmlund, H. Huomo, J. M. Illiano, P. Jensen, M. A. Johnson, D. R. Linder, T. Lun-
 694 tama, S. Maurice, K. P. McCabe, K. Mursula, B. T. Narheim, J. E. Nordholt, A. Preece,
 695 J. Rudzki, A. Ruitberg, K. Smith, S. Szalai, M. F. Thomsen, K. Viherkanto, J. Vilp-
 696 pola, T. Vollmer, T. E. Wahl, M. Wüest, T. Ylikorpi, and C. Zinsmeyer (2004), Cassini
 697 Plasma Spectrometer investigation, *Space Science Reviews*.
- 698 Young, D. T., J.-J. Berthelier, M. Blanc, J. L. Burch, S. Bolton, A. J. Coates, F. J.
 699 Crary, R. Goldstein, M. Grande, T. W. Hill, R. E. Johnson, R. A. Baragiola, V. Kelha,
 700 D. J. McComas, K. Mursula, E. C. Sittler, K. R. Svenes, K. Szegö, P. Tanskanen,
 701 M. F. Thomsen, S. Bakshi, B. L. Barraclough, Z. Bebesi, D. Delapp, M. W. Dun-
 702 lop, J. T. Gosling, J. D. Furman, L. K. Gilbert, D. Glenn, C. Holmlund, J.-M. Illiano,
 703 G. R. Lewis, D. R. Linder, S. Maurice, H. J. McAndrews, B. T. Narheim, E. Pallier,
 704 D. Reisenfeld, A. M. Rymer, H. T. Smith, R. L. Tokar, J. Vilppola, and C. Zinsmeyer
 705 (2005), Composition and Dynamics of Plasma in Saturn's Magnetosphere, *Science*, 307,
 706 1262–1266, doi:10.1126/science.1106151.

Figure 1.

Author Manuscript

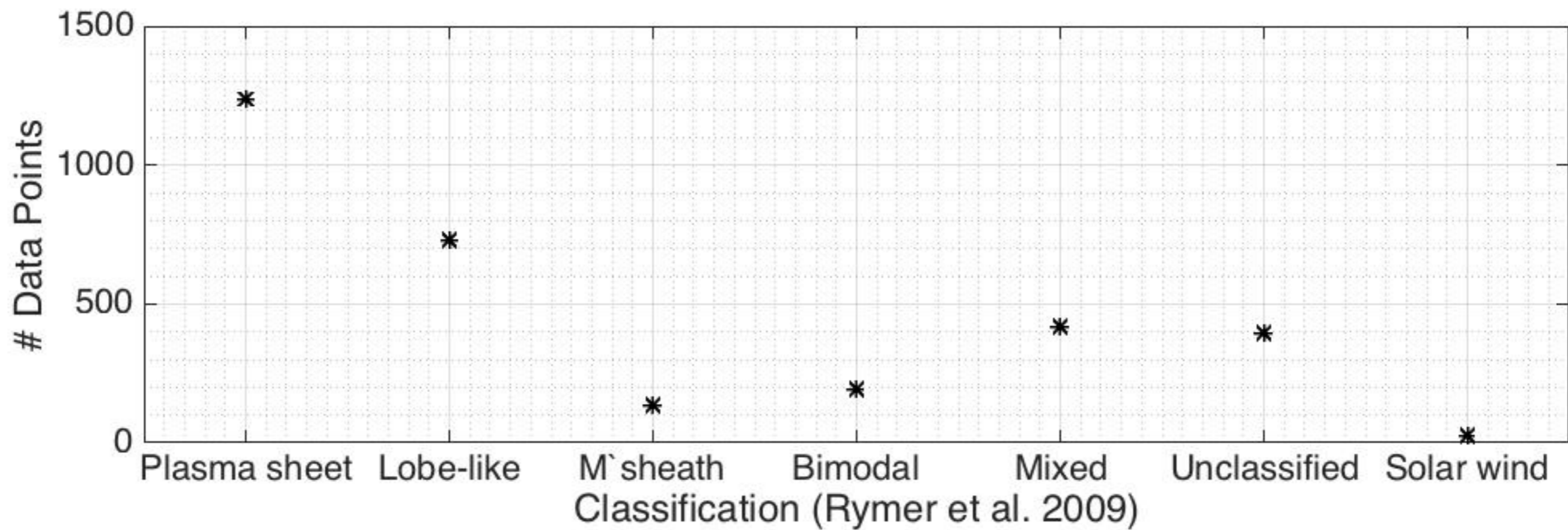
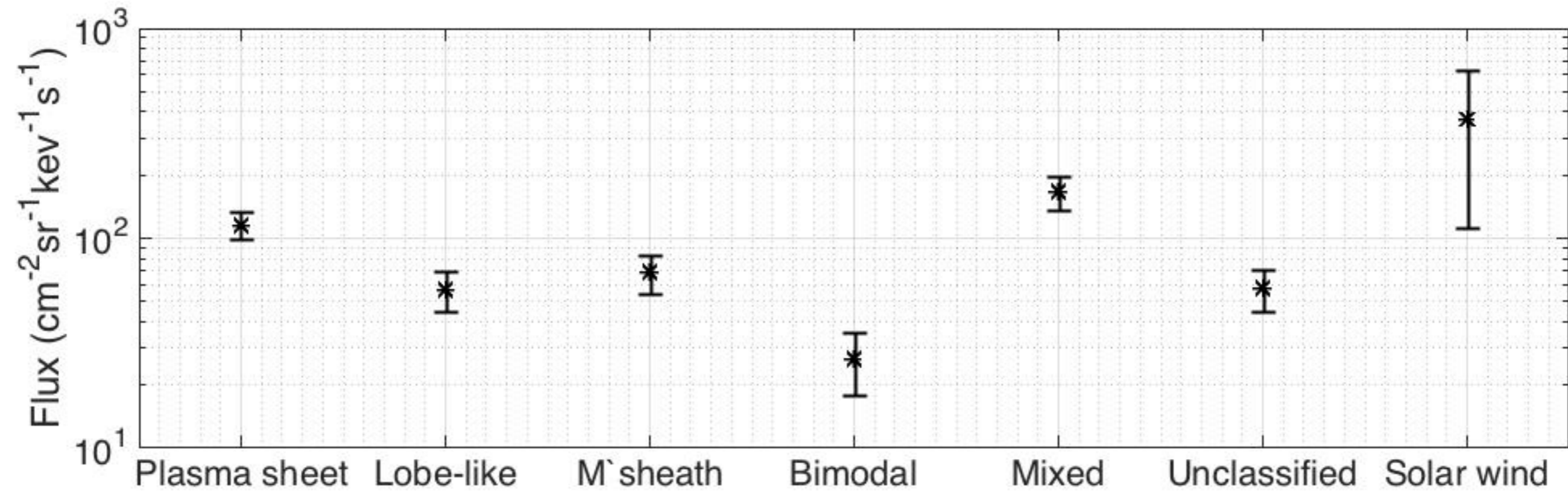
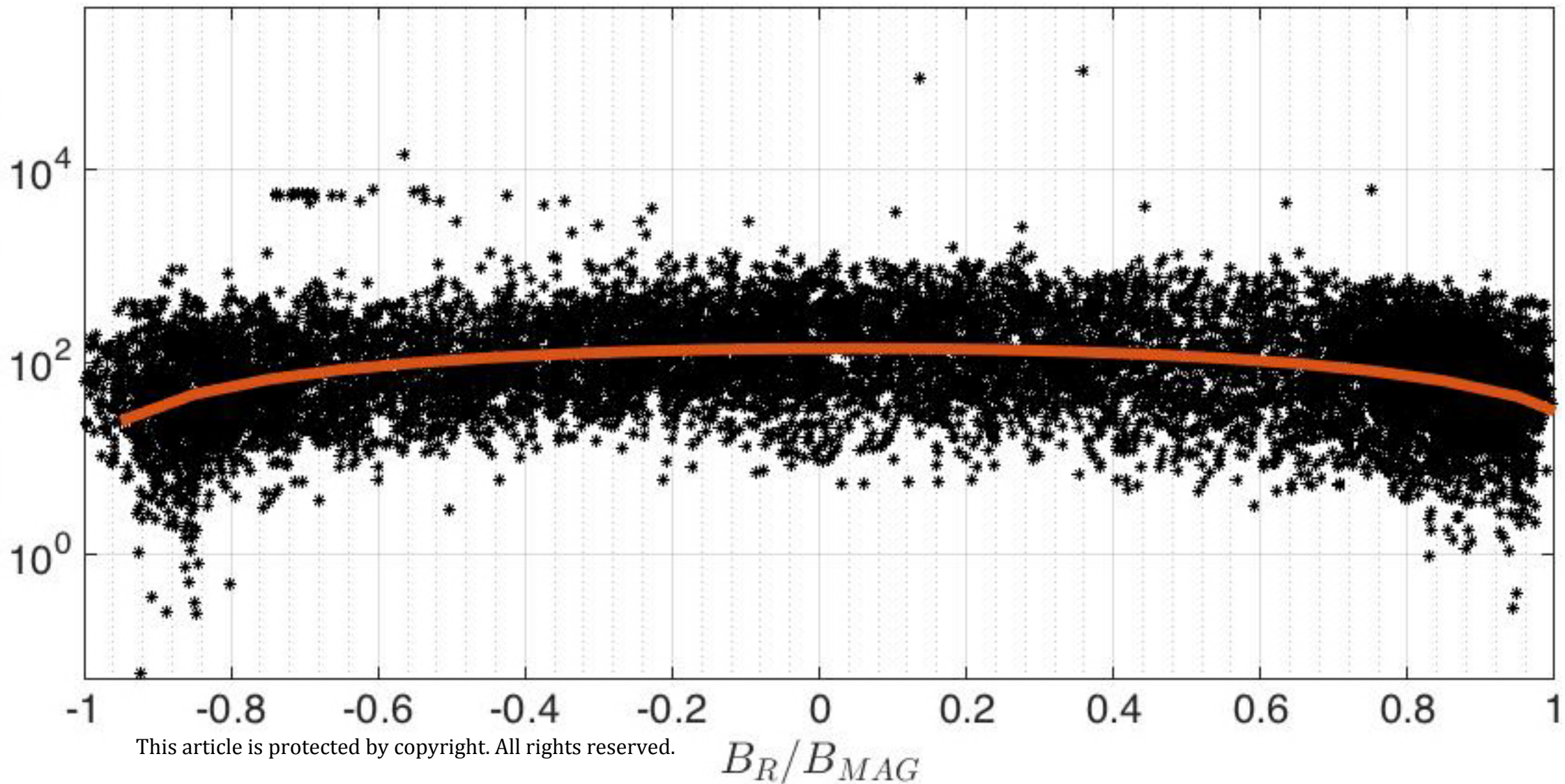


Figure 2.

Author Manuscript



This article is protected by copyright. All rights reserved.

B_R/B_{MAG}

Figure 3.

Author Manuscript

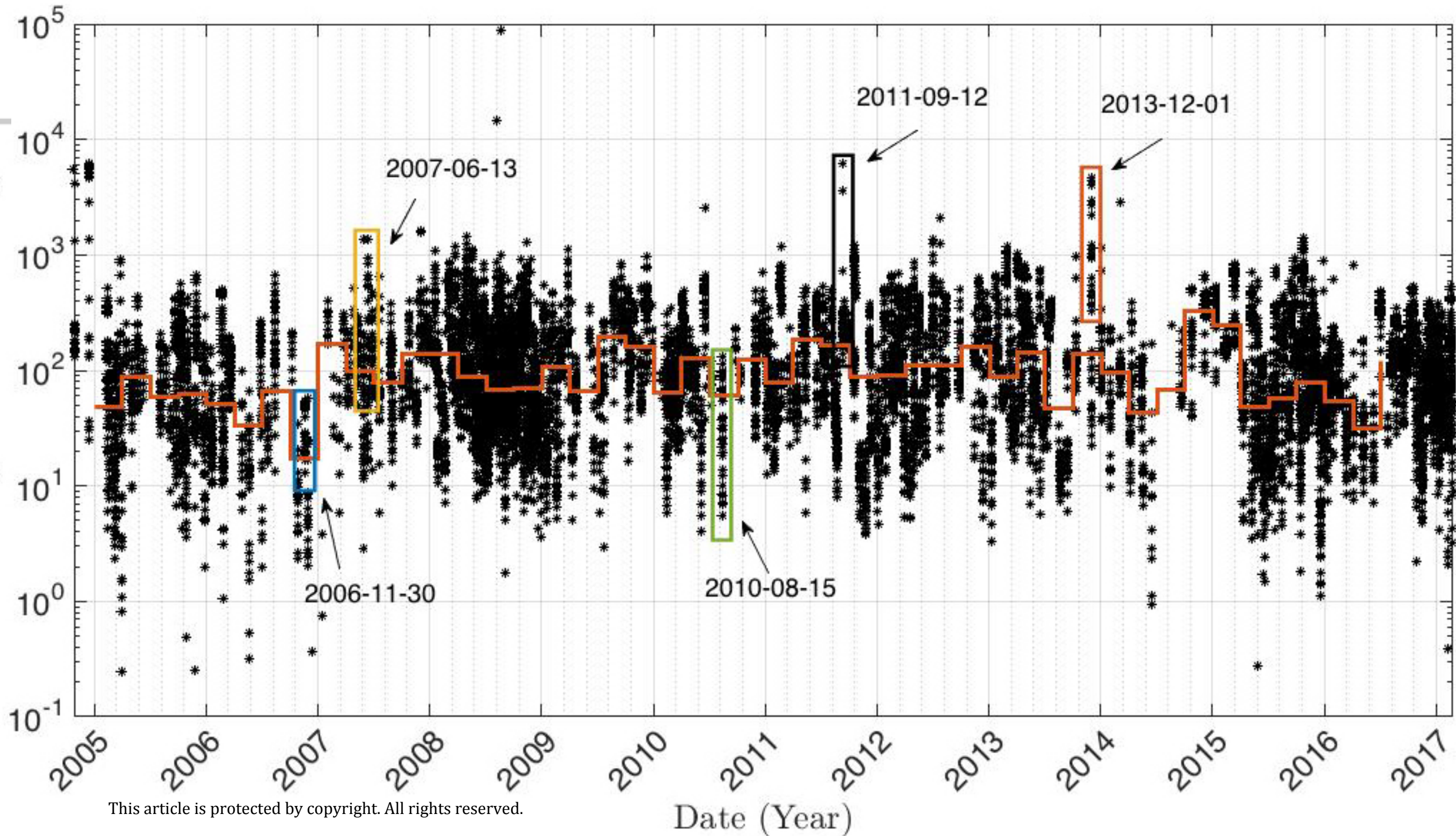
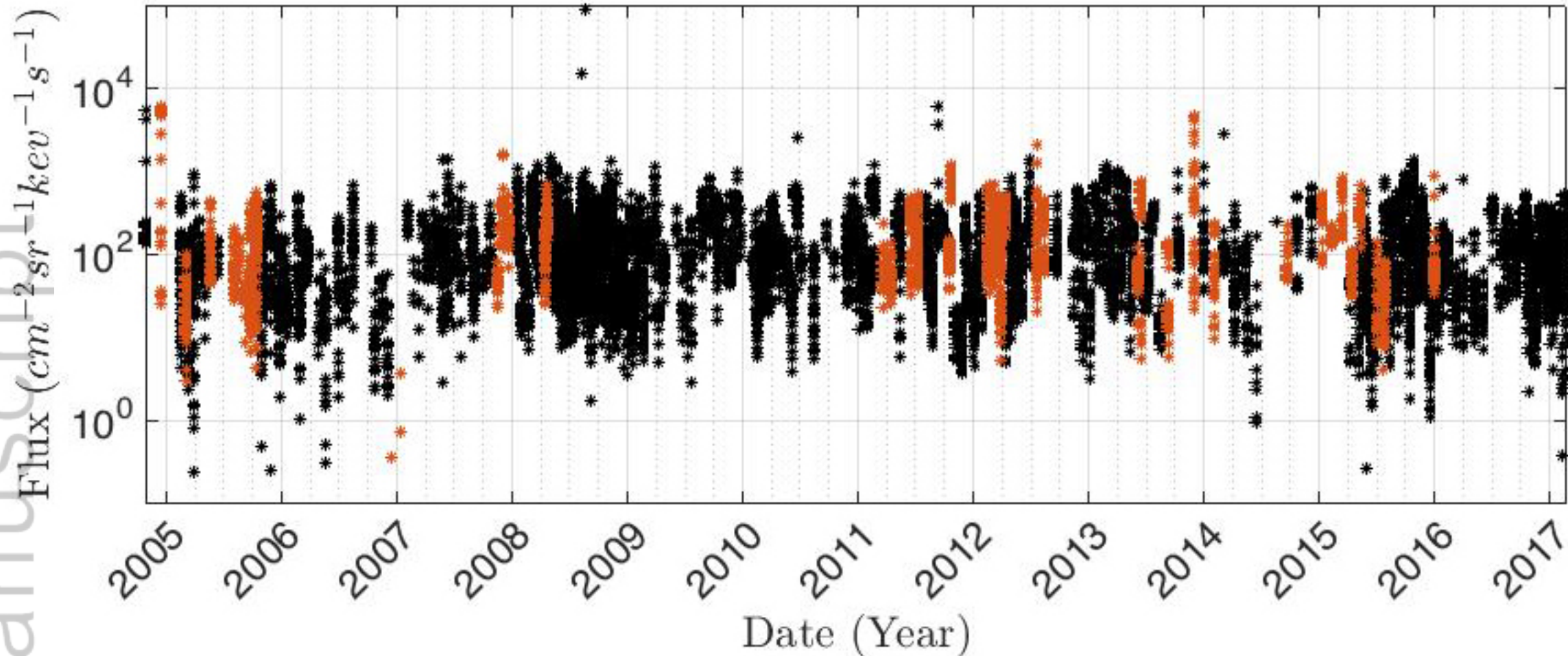


Figure 4.

Author Manuscript

A0 channel (27-35 keV)



A5 channel (506-805 keV)

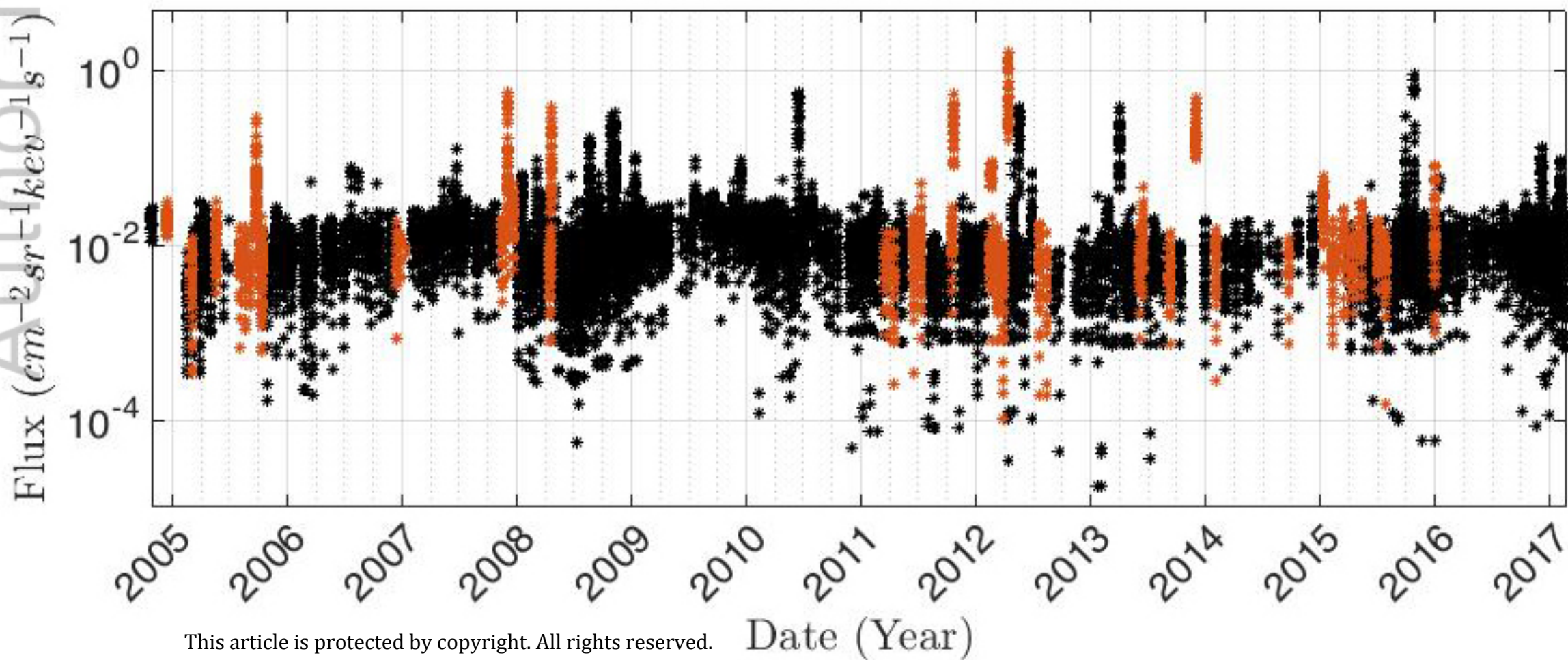


Figure 5.

Author Manuscript

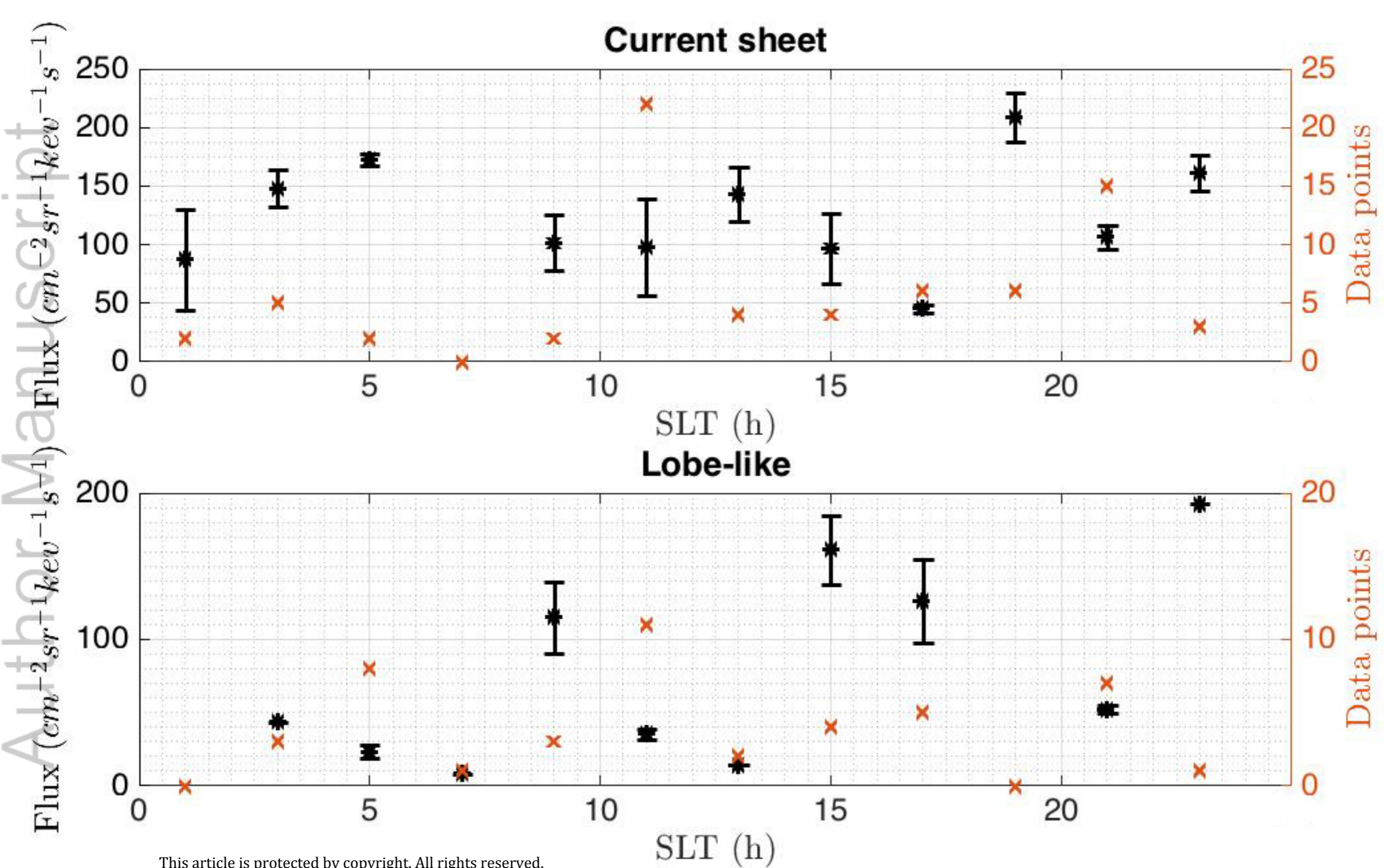
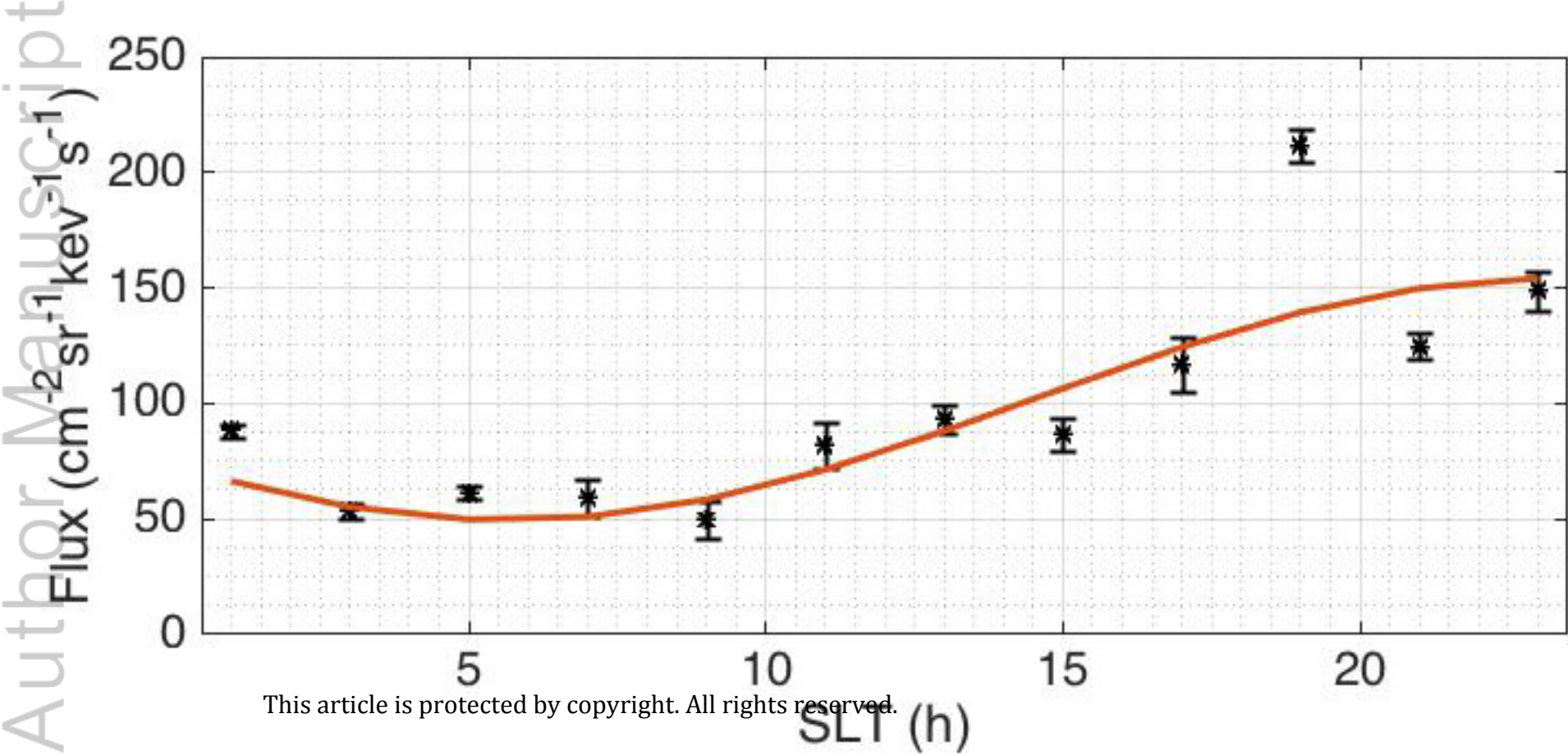


Figure 6.

Author Manuscript

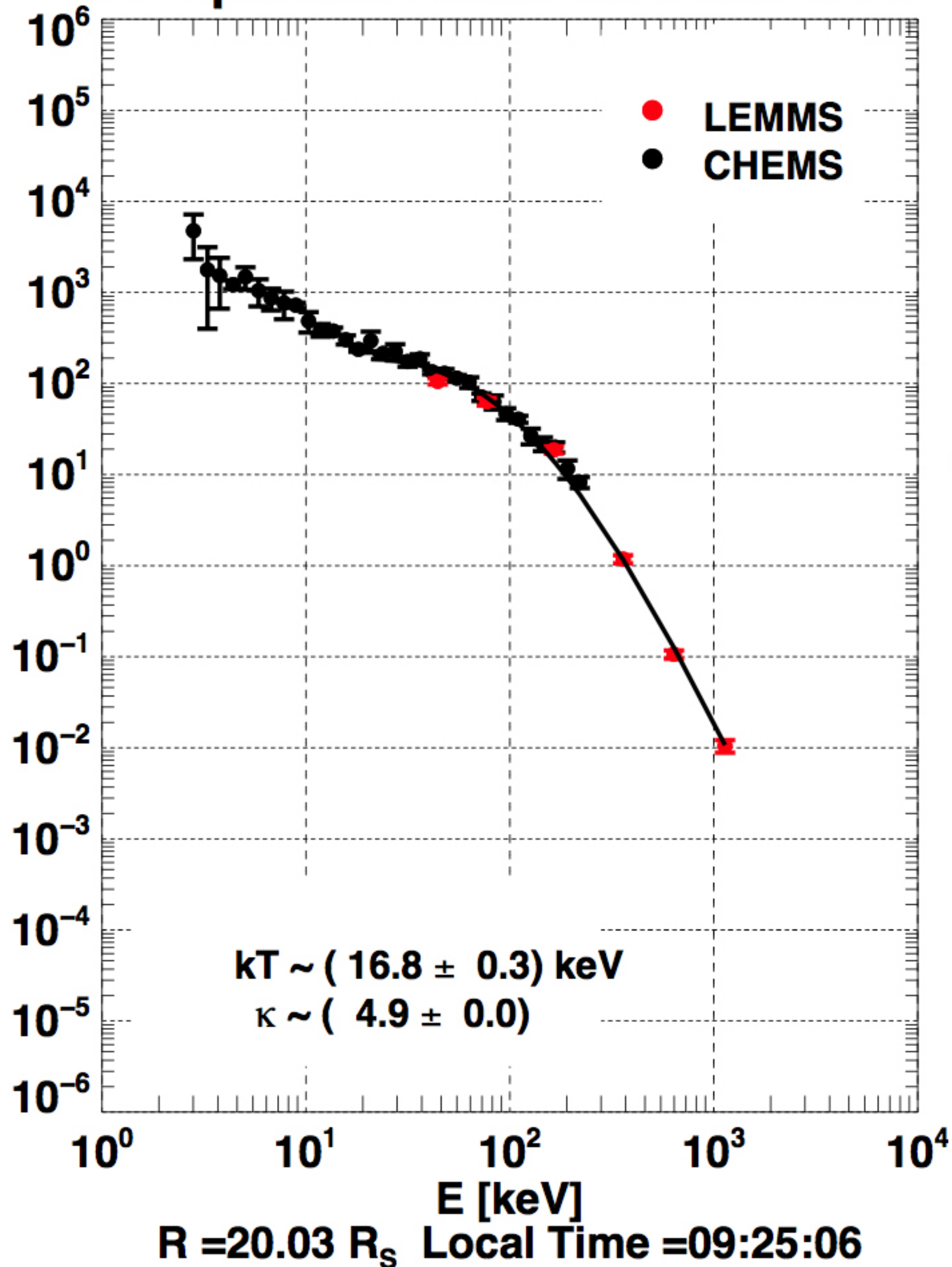


This article is protected by copyright. All rights reserved.

Figure 7.

Author Manuscript

H⁺ Spectra: 2005/265 04:05 UTC



H⁺ Spectra: 2012/103 23:02 UTC

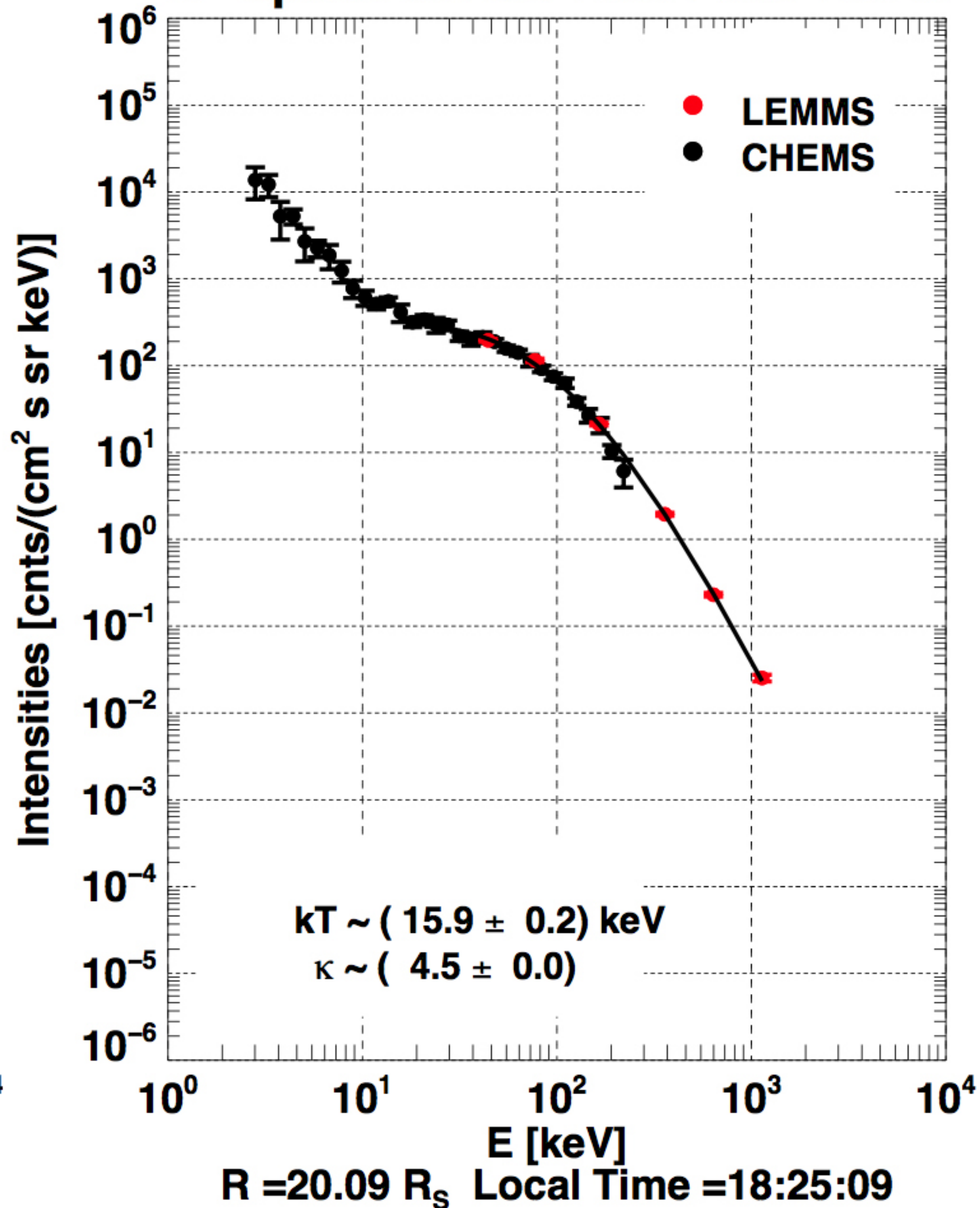


Figure 8.

Author Manuscript

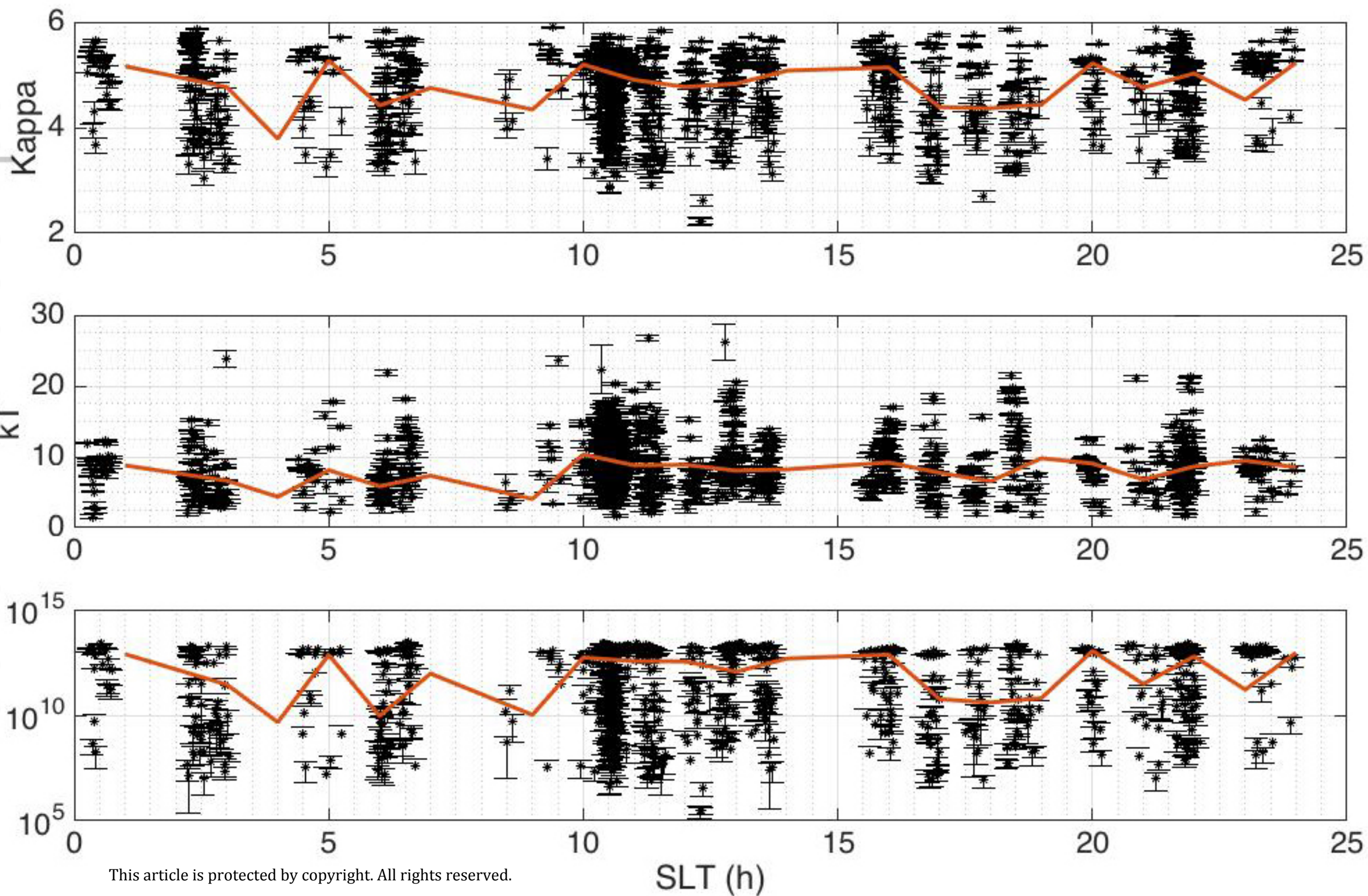
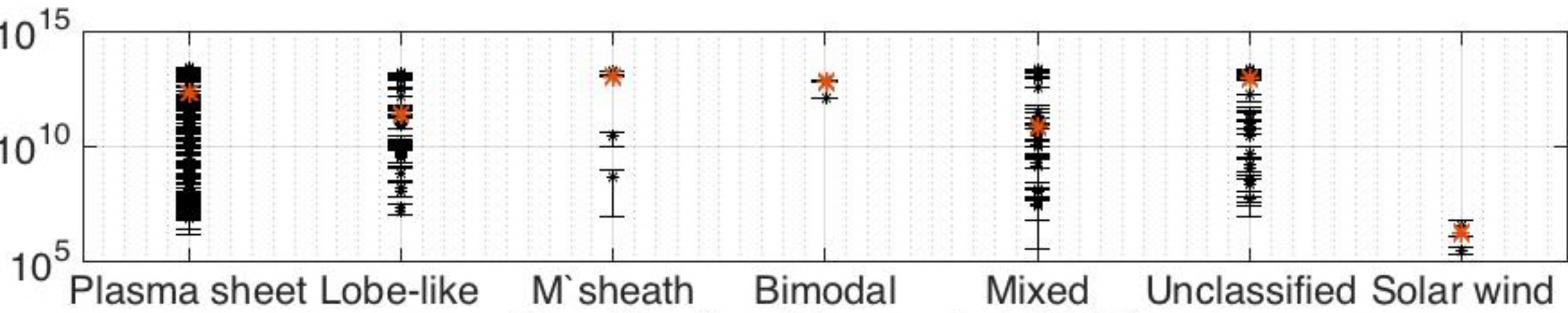
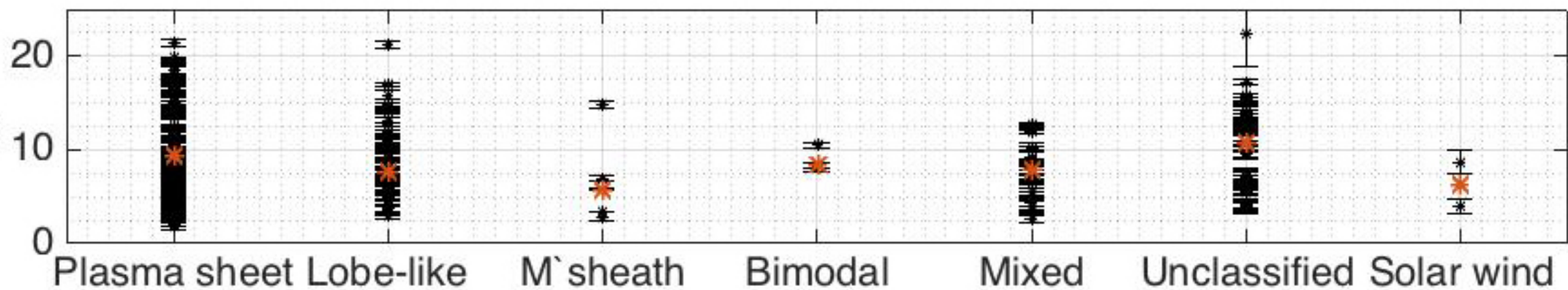
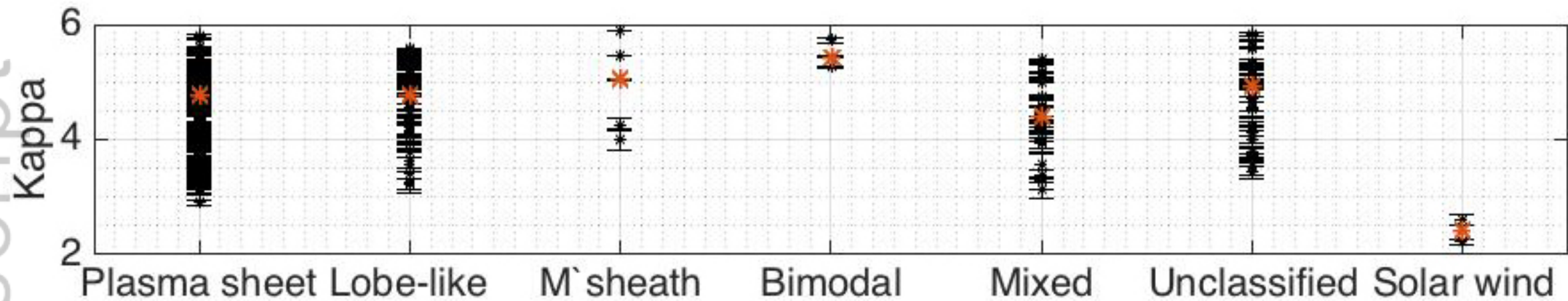
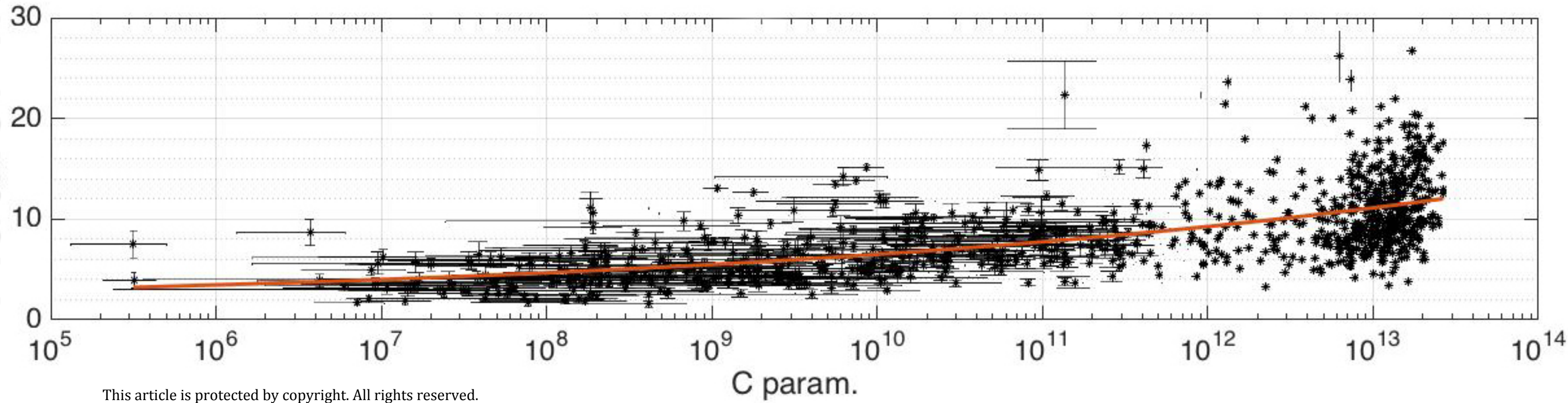
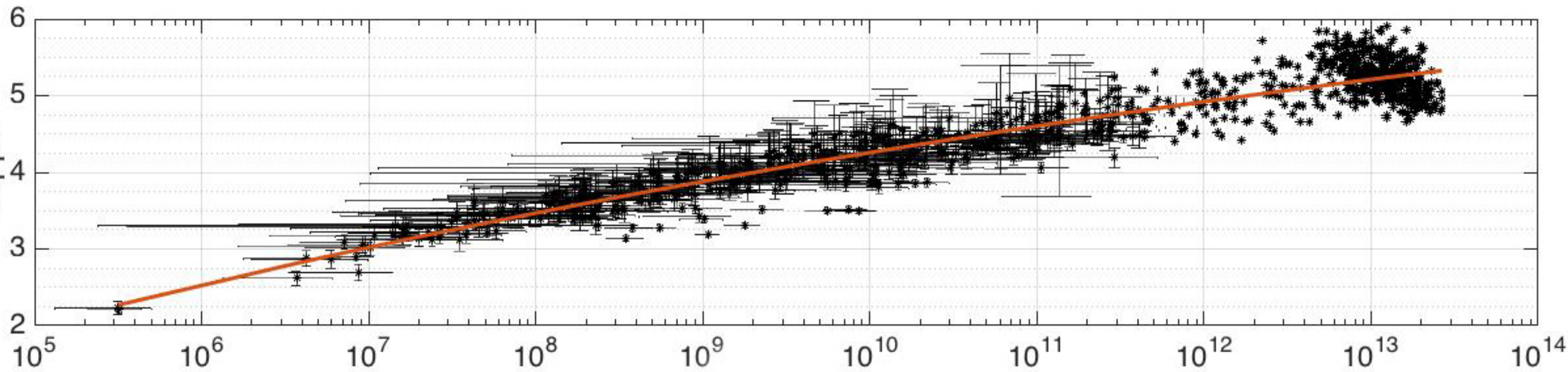
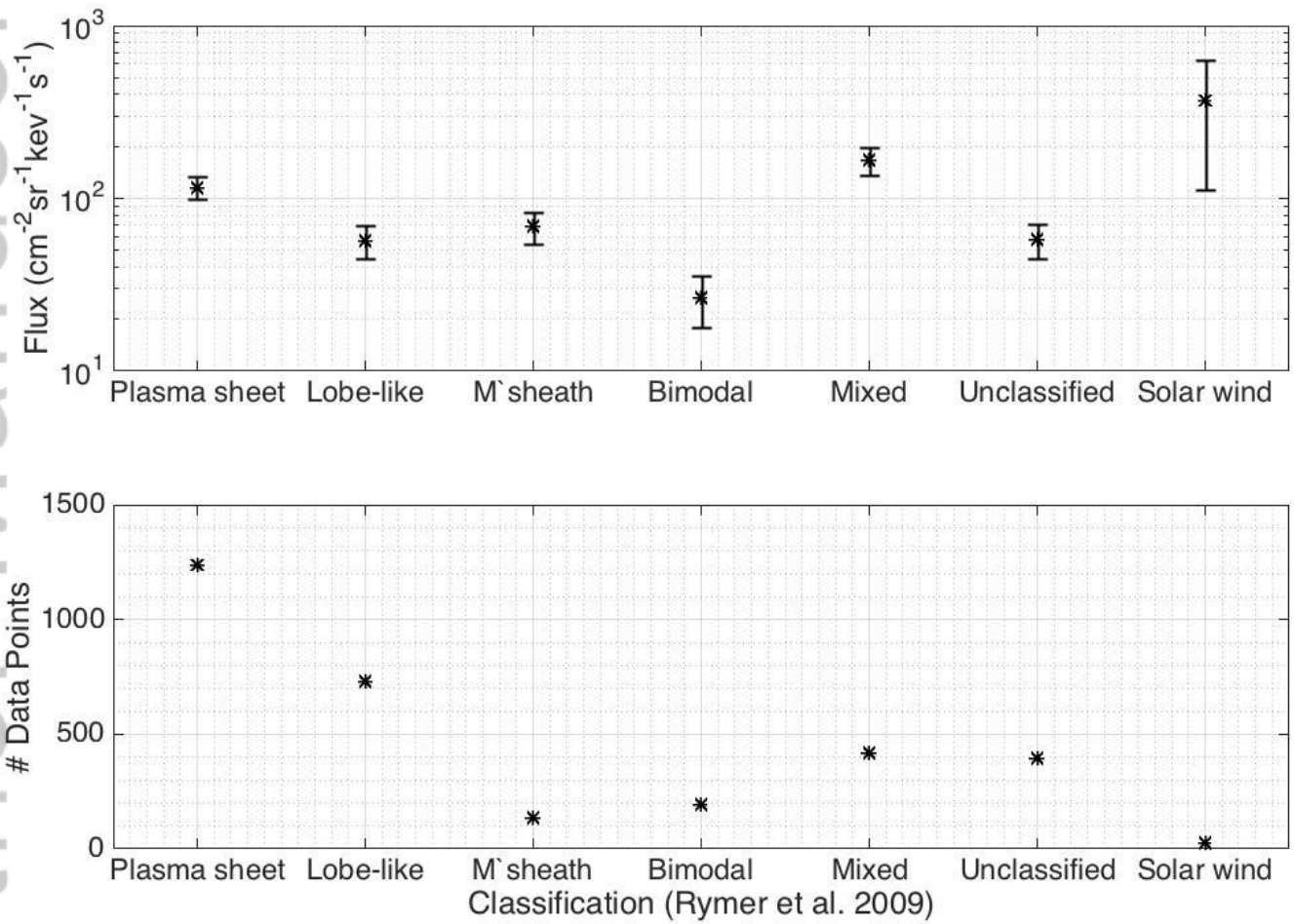


Figure 9.

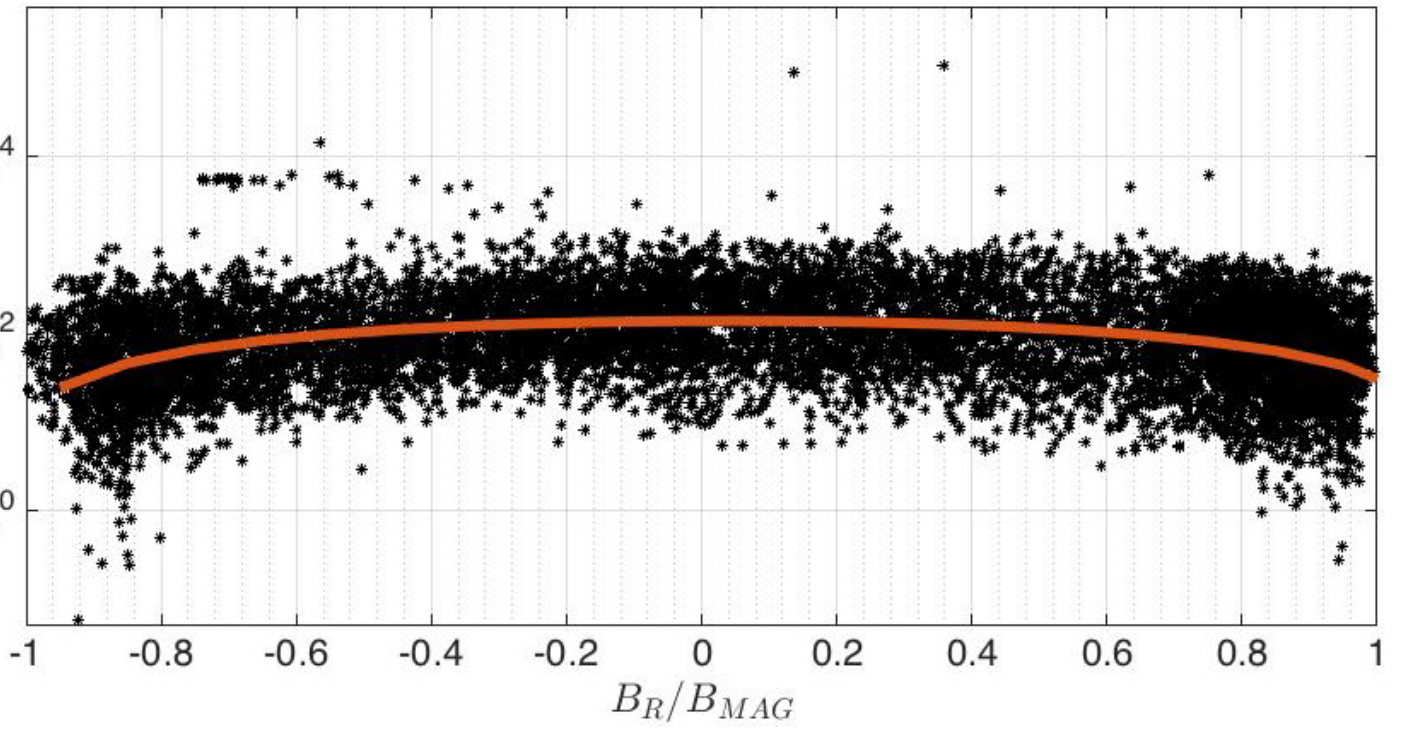
Author Manuscript



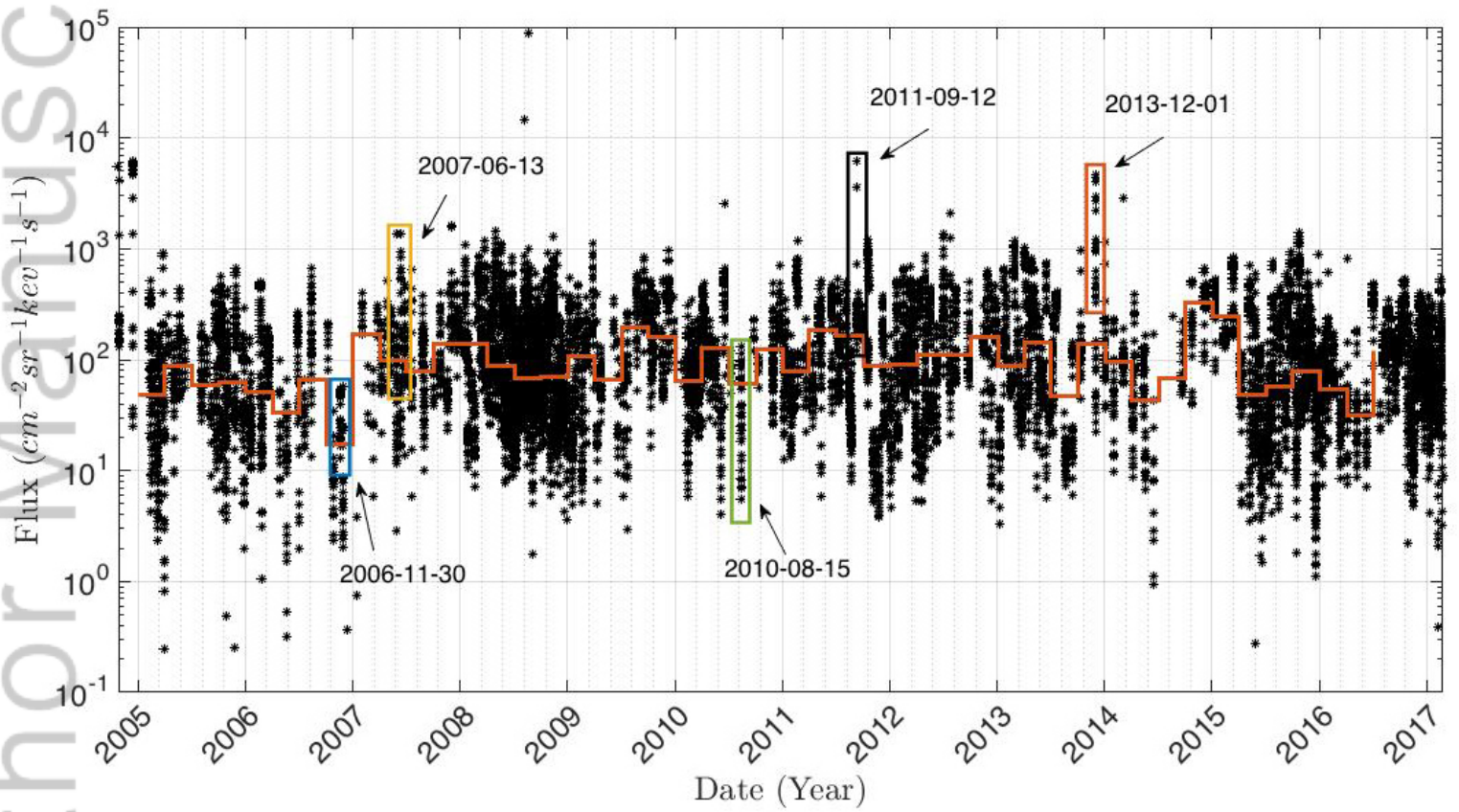




2018JA025442-f01-z-.jpg

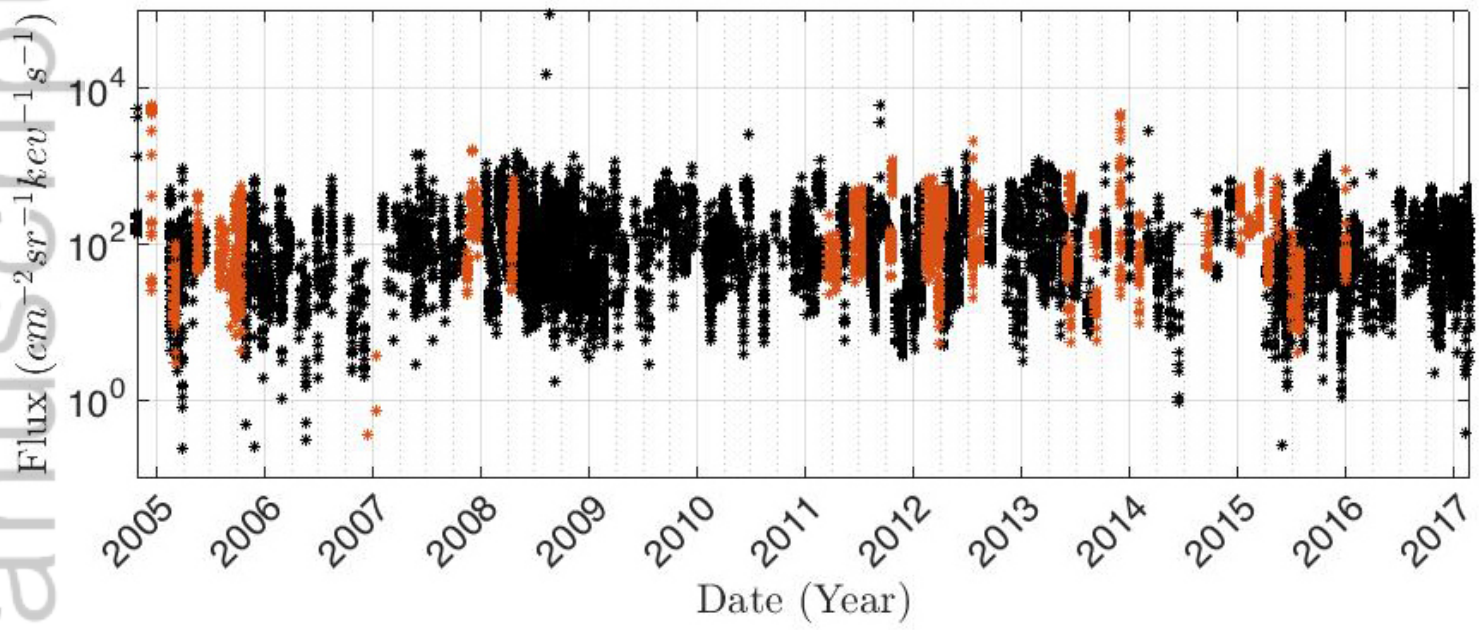


2018JA025442-f02-z-.jpg

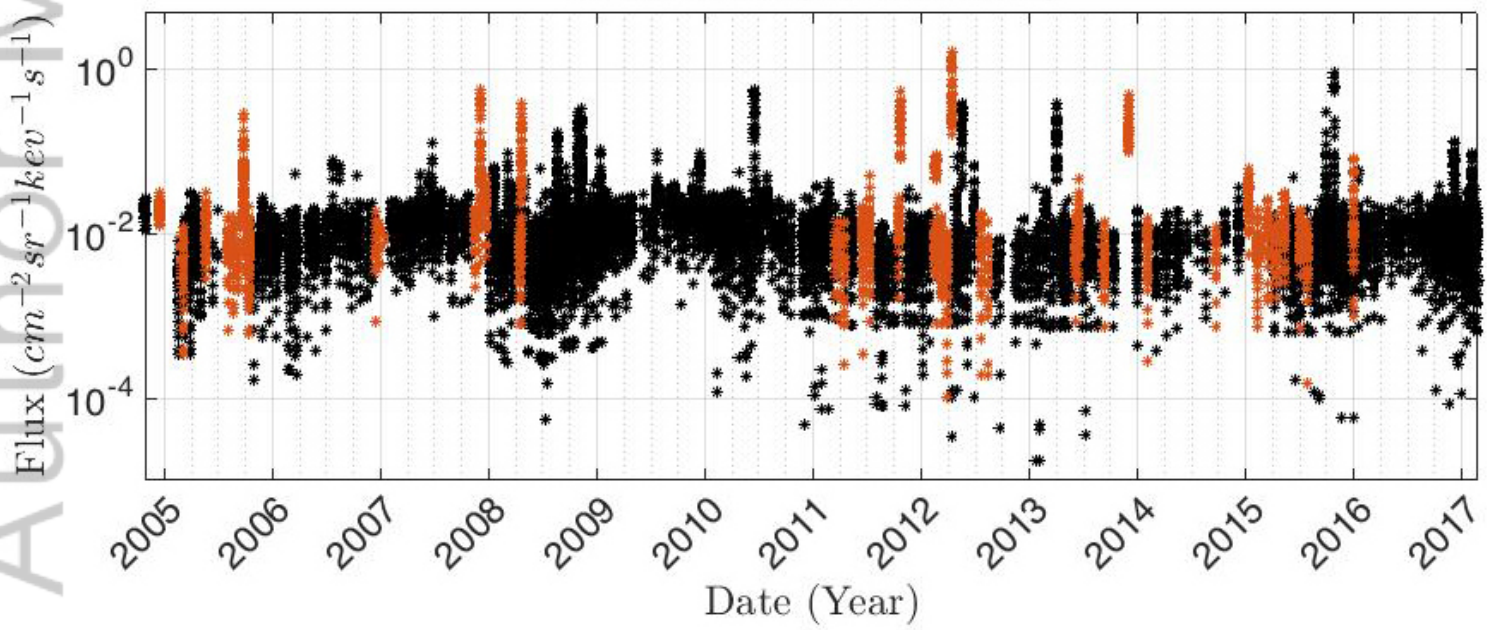


2018JA025442-f03-z.jpg

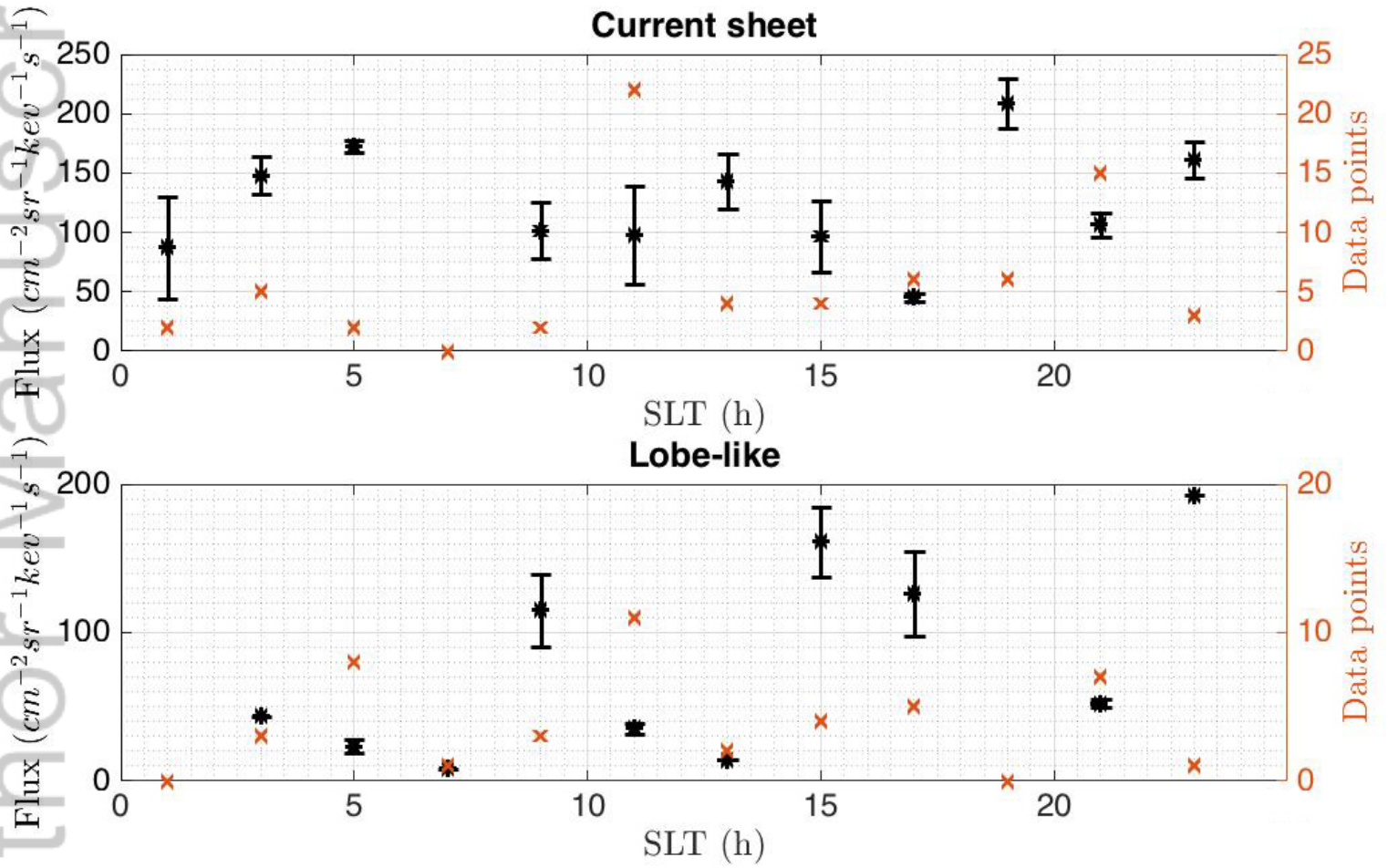
A0 channel (27-35 keV)



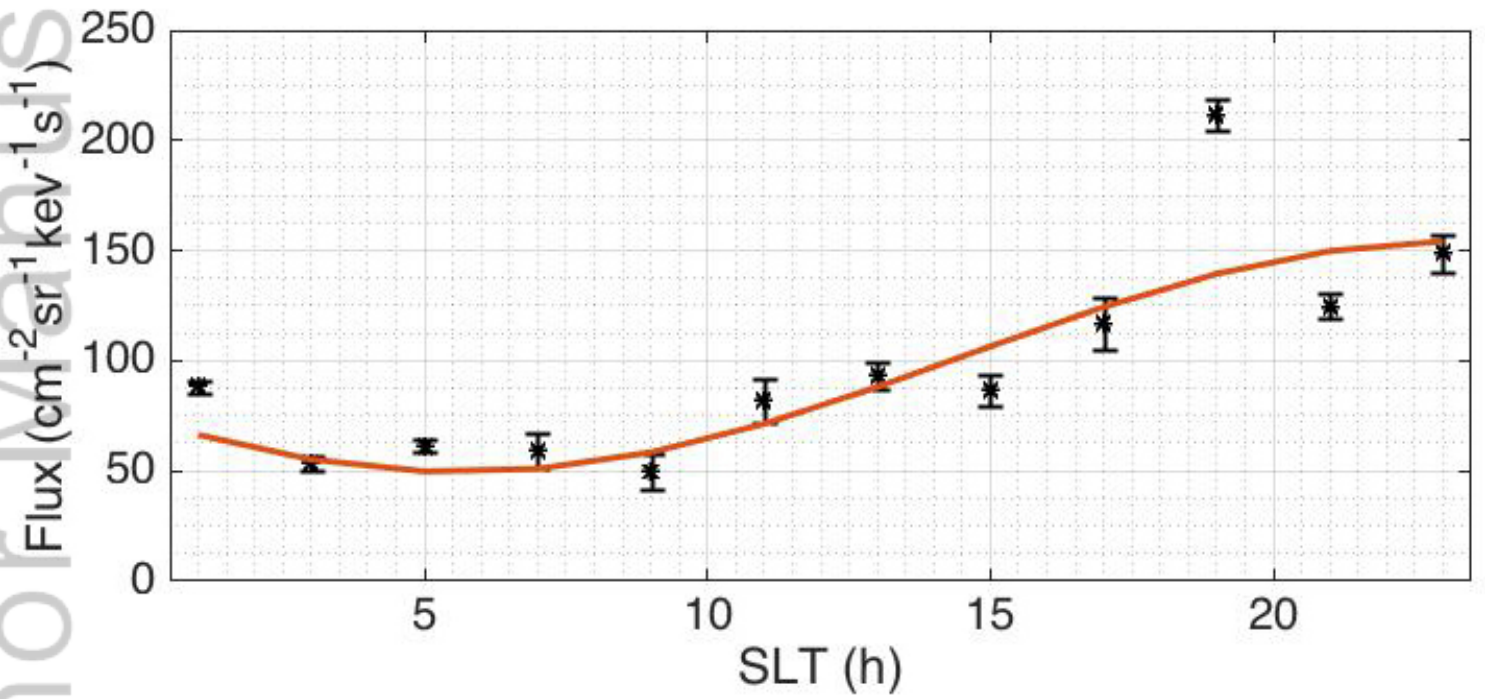
A5 channel (506-805 keV)



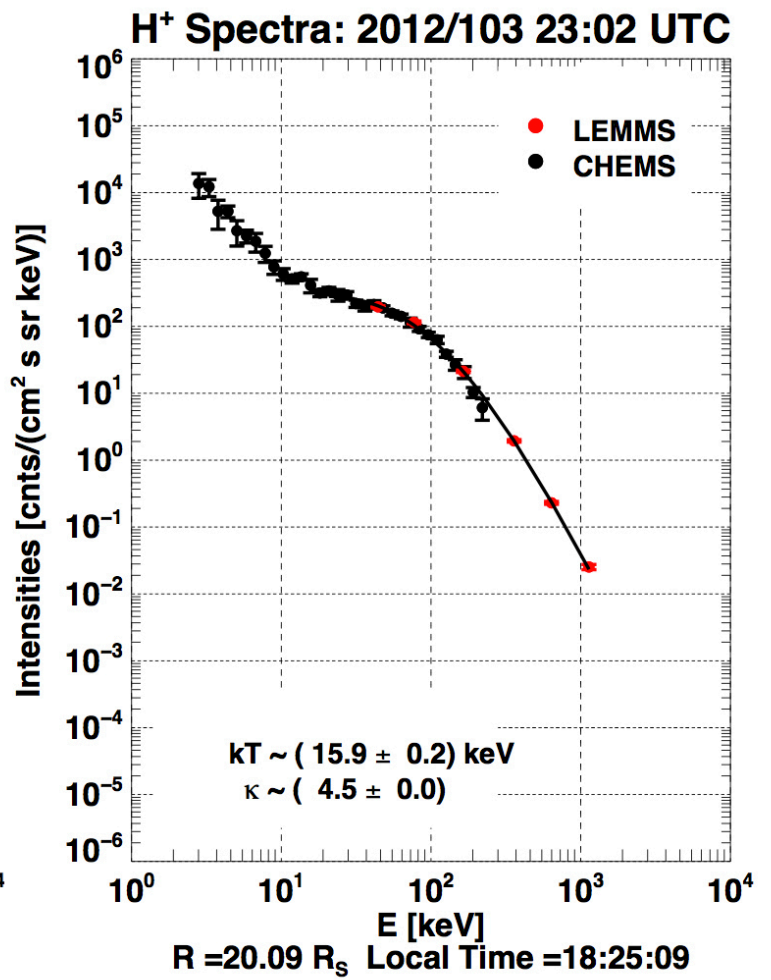
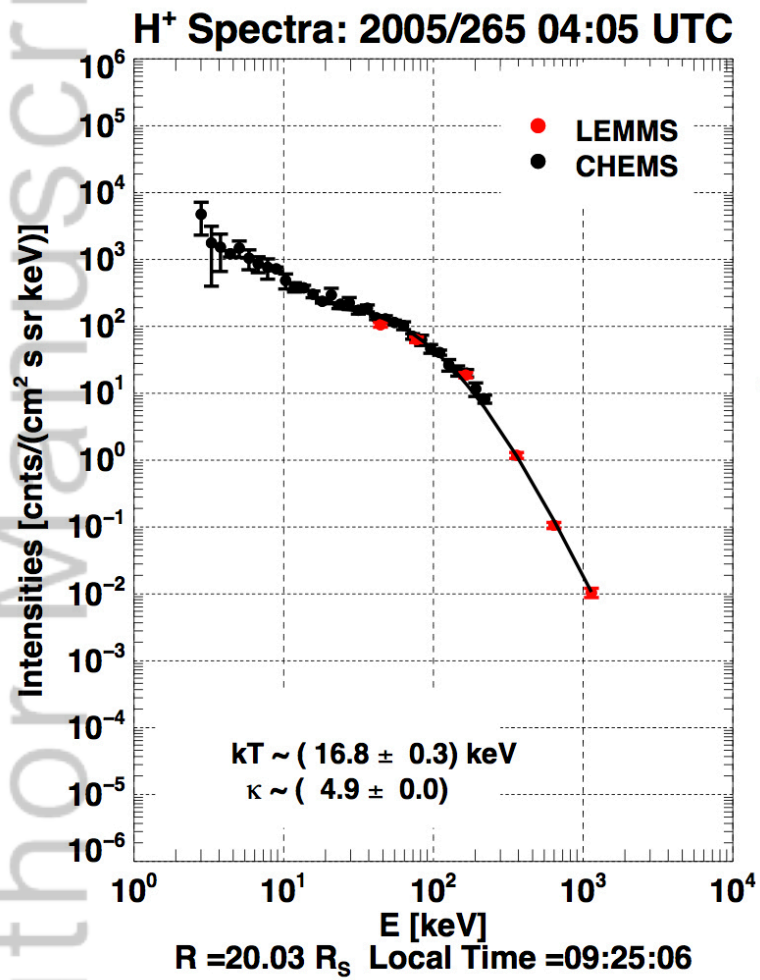
2018JA025442-f04-z-.jpg



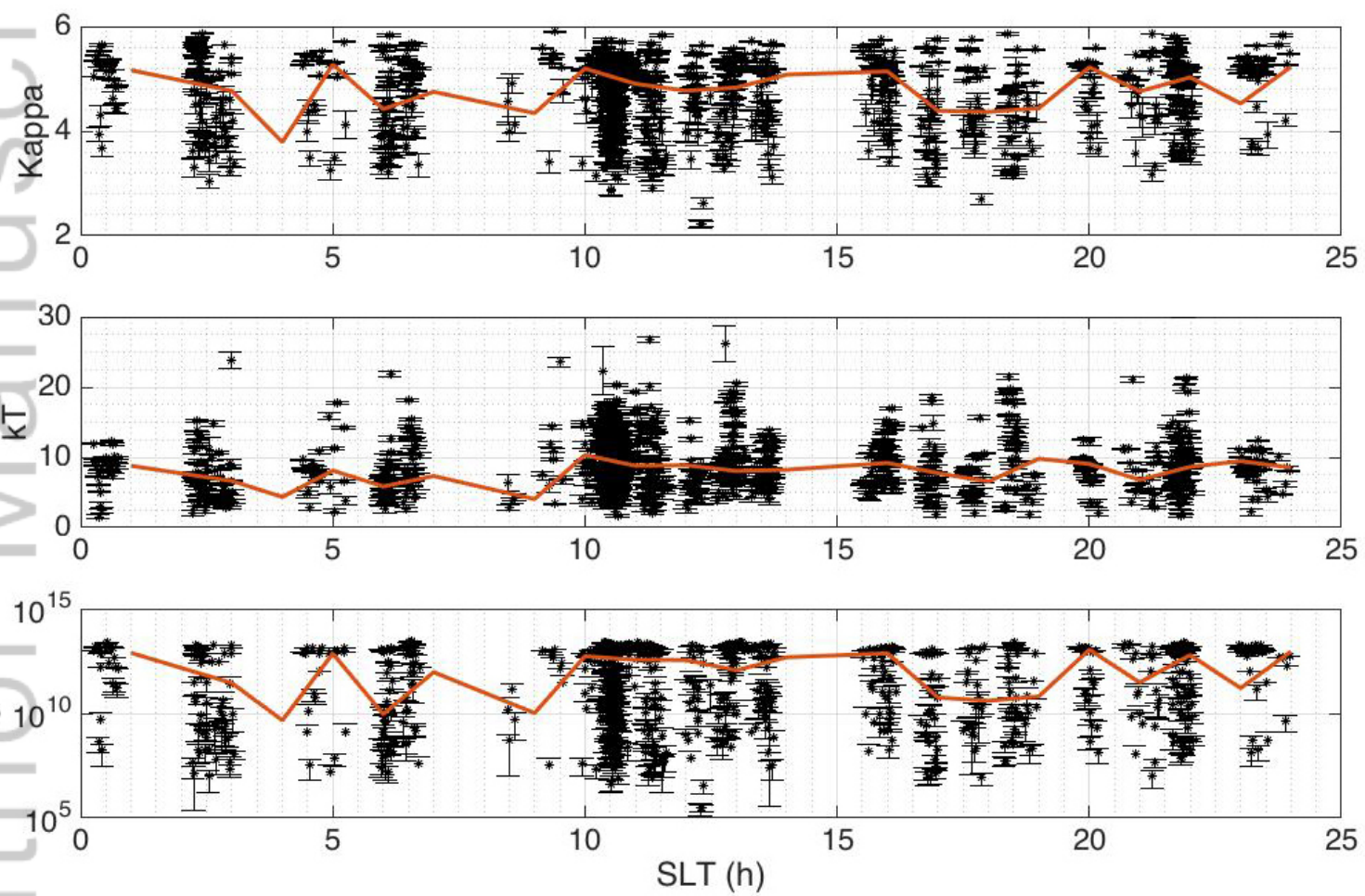
2018JA025442-f05-z-jpg



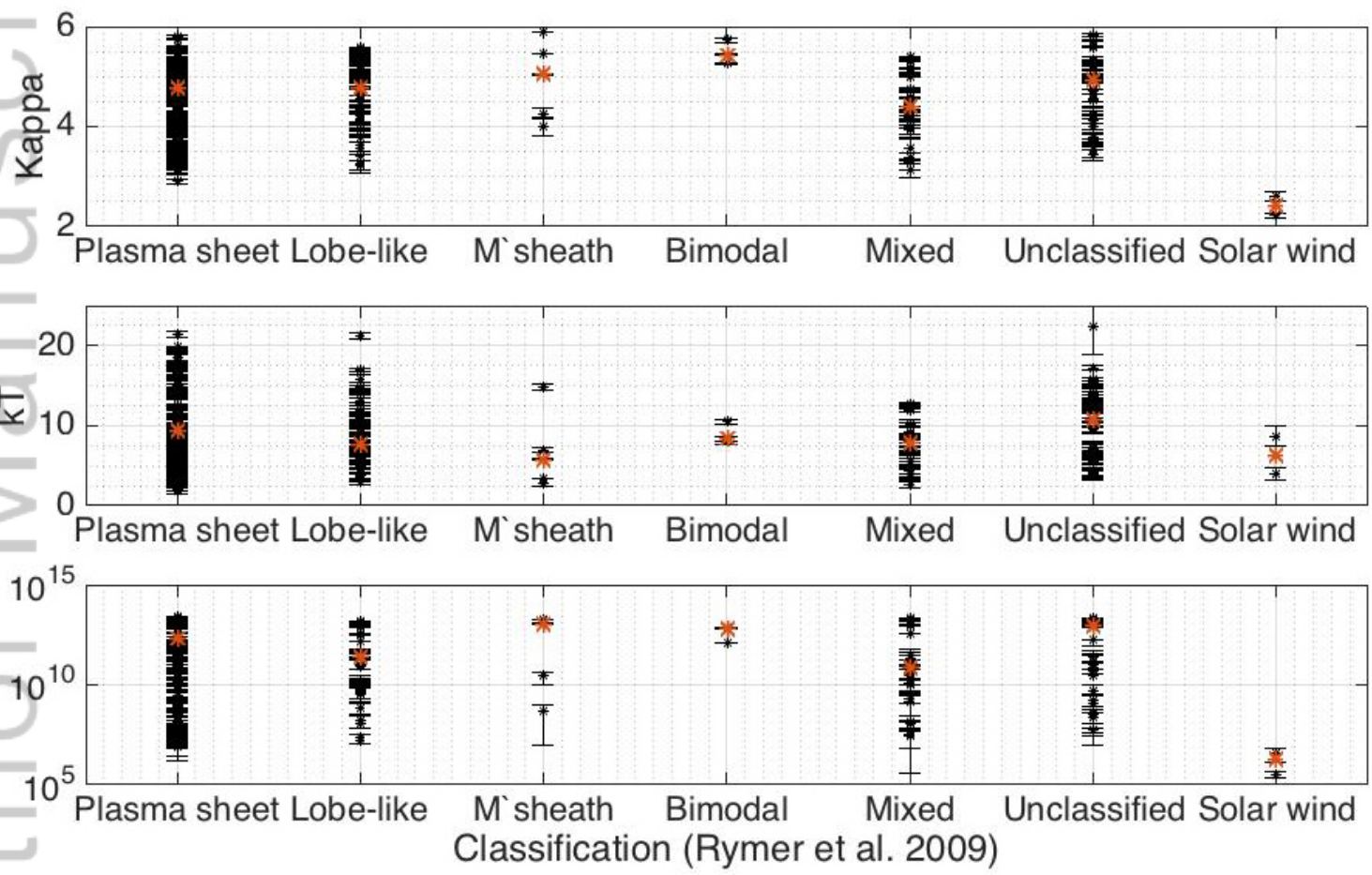
2018JA025442-f06-z-.jpg



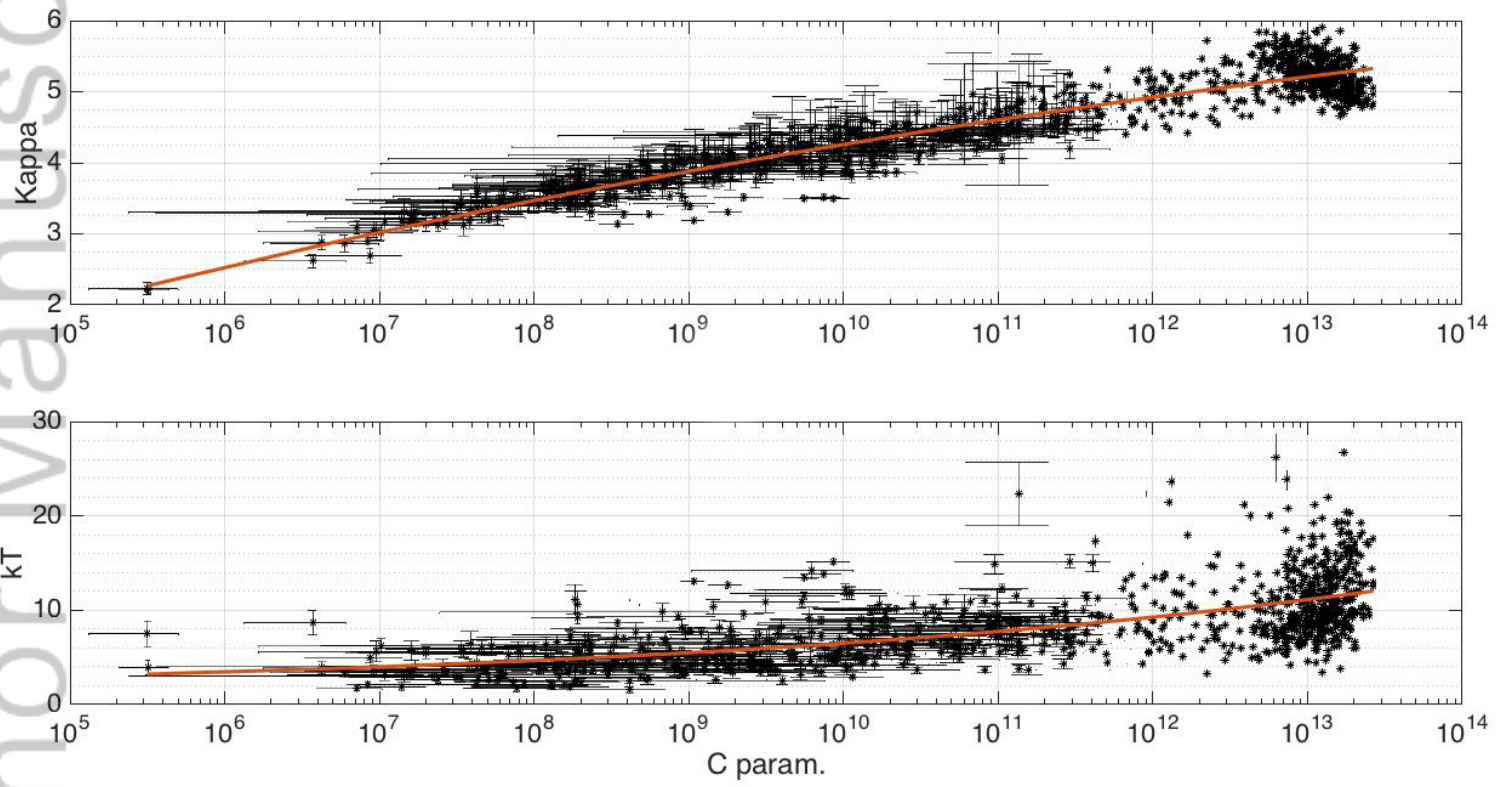
2018JA025442-f07-z-.jpg



2018JA025442-f08-z-jpg



2018JA025442-f09-z-.jpg



2018JA025442-f10-z-.jpg